Source attribution of black carbon and its direct radiative forcing in China

Yang Yang[1], Hailong Wang[1*], Steven J. Smith[2], Po-Lun Ma[1], Philip J. Rasch[1]

[1]Atmospheric Science and Global Change Division, Pacific Northwest National Laboratory, Richland, Washington, USA

[2]Joint Global Change Research Institute, Pacific Northwest National Laboratory, College Park, Maryland, USA

*Correspondence to yang.yang@pnnl.gov and hailong.wang@pnnl.gov

Abstract

The source attributions for mass concentration, haze formation, transport, and direct radiative forcing of black carbon (BC) in various regions of China are quantified in this study using the Community Earth System Model (CESM) with a source-tagging technique. Anthropogenic emissions are from the Community Emissions Data System that is newly developed for the Coupled Model Intercomparison Project Phase 6 (CMIP6). Over North China where the air quality is often poor, about 90% of near-surface BC concentration is contributed by local emissions. 35% of BC concentration over South China in winter can be attributed to emissions from North China and 19% comes from sources outside China in spring. For other regions in China, BC is largely contributed from non-local sources. We further investigated potential factors that contribute to the poor air quality in China. During polluted days, a net inflow of BC transported from non-local source regions associated with anomalous winds plays an important role in increasing local BC concentrations. BC-containing particles emitted from East Asia can also be transported across the Pacific. Our model results show that emissions from inside and outside China are equally important for the BC outflow from East Asia, while emissions from China account for 8% of BC concentration and 29% in column burden in western United States in spring. Radiative forcing estimated shows that 65% of the annual mean BC direct radiative forcing (2.2 W m^{-2}) in China results from local emissions, and the remaining 35% are contributed by emissions outside of China. Efficiency analysis shows that reduction in BC emissions over eastern China could benefit more on the regional air quality in China, especially in winter haze season.

1. Introduction

Black carbon (BC), as a component of atmospheric fine particulate matter ($PM_{2.5}$), is harmful to human health (Anenberg et al., 2011; Janssen et al., 2012). In addition to its impact on air quality, as the most efficient light-absorbing anthropogenic aerosols, BC is thought to exert a substantial influence on climate (Bond et al., 2013; IPCC, 2013; Liao et al., 2015). It can heat the atmosphere through absorbing solar radiation (Ramanathan and Carmichael, 2008), influence cloud microphysical and dynamical processes (Jacobson, 2006; McFarquhar and Wang, 2006), and reduce surface albedo through deposition on snow and ice (Flanner et al., 2007; Qian et al., 2015).

Due to accelerated urbanization and rapid economic growth, emissions of BC in China increased dramatically during recent decades. It contributed to about one fourth of the global emissions of BC in recent decades (Bond et al., 2007). Strong emissions lead to high concentrations of BC over China. Zhang et al. (2008) collected aerosol samples at eighteen stations spread over China during 2006 and reported BC concentrations in a range of 9–14 μg m^{-3} at urban sites, 2–5 μg m^{-3} at rural sites, and about 0.35 μg m^{-3} at remote background sites. BC also exerts significant positive direct radiative forcing (DRF) at the top of the atmosphere (TOA) in China. Using the Regional Climate Chemistry Modeling System (RegCCMs), Zhuang et al. (2013) reported an annual mean BC DRF of 2–5 W m^{-2} at TOA over eastern China and about 6 W m^{-2} over Sichuan Basin in year 2006. Li et al. (2016) also showed a strong DRF of BC over the North China Plain and Sichuan Basin in most seasons except for spring when the strongest BC DRF with values of 4–6 W m^{-2} shifted to southern China.

BC is the product of incomplete combustion of fossil fuels, biofuels, and open burning, such as forest and grassland fires and agricultural waste burning on fields. In the atmosphere the average lifetime of BC is only a few days, due to both wet removal and dry deposition, which is much shorter than that of long-lived greenhouse gases. In addition, BC lifetime is region dependent. BC in East Asia has a shorter lifetime than the global mean value due to a faster regional removal (H. Wang et al.,

2014), probably associated with strong precipitation during monsoon season. BC emission reductions may benefit both mitigation of global climate change and regional air quality (Shindell et al., 2012; Bond et al., 2013; Smith and Mizrahi, 2013), especially in East Asia where fuel combustion emits substantial BC along with other pollutant species. Many previous observational and/or modeling studies have examined the source sector contributions of BC over China (Zhuang et al., 2014; Y.-L. Zhang et al., 2015; Li et al., 2016). They found that residential heating and industry sectors were the largest contributors to BC concentrations in China, while biomass burning emissions from outside China were important to BC in western China. An effective BC reduction in a receptor region would require knowing not only the source sector that contributes the most to BC levels, but also the source contributions from various locations within and outside the region. However, very few previous studies have focused on the source attribution of BC concentrations in various regions of China. Li et al. (2016) examined the contributions of emissions inside and outside China to BC over China (with only two source regions) but did not divide the source contributions from different regions inside China.

Pollution levels also show substantial daily to weekly variation. In recent years, extreme wintertime hazy conditions occurred frequently in China and caused serious air pollution, affecting more than half of the 1.3 billion people (Ding and Liu, 2014). During one winter haze episode in 2013, BC concentrations increased up to about 20 and 8 μg m^{-3} in Xi'an and Beijing over northern China, and 6 and 4 μg m^{-3} in Guangzhou and Shanghai over southern China, respectively (Y.-L. Zhang et al., 2015). The transport of pollutants from upwind was reported to be one of the most important contributors to local high aerosol concentrations during haze days (L. T. Wang et al., 2014; Y. Yang et al., 2016). L. T. Wang et al. (2014) found that emissions from northern Hebei and Beijing-Tianjin were the major contributor to particulate matter ($PM_{2.5}$) pollution in Shijiazhuang in January 2013. Yang et al. (2016) confirmed a connection between wind fields and $PM_{2.5}$ concentrations during winter hazy days through model simulations and statistical analysis. They also found that weakened winds contributed to increases in winter aerosol concentrations and hazy days over

eastern China during recent decades. As a chemically inert species, atmospheric BC is a good tracer to investigate the source region contributions from local and non-local emissions during polluted conditions that are related to long-range transport.

BC particles originating from East Asia can also be transported across the North Pacific, reaching North America (Hadley et al., 2007; Ma et al., 2013a; Matsui et al., 2013; H. Wang et al., 2014; Yang et al., 2015). Matsui et al. (2013) simulated outflow of BC from East Asia using the Community Multiscale Air Quality (CMAQ) model and found that anthropogenic emissions from China, biomass burning emissions from Southeast Asia, and biomass burning emissions from Siberia and Kazakhstan contributed 61%, 17%, and 6%, respectively, to the eastward BC flux at 150°E averaged over 2008–2010. Hadley et al. (2007) estimated the trans-Pacific transport of BC during April of 2004 using the Chemical Weather Forecast System (CFORS) model and reported that, across 130°W, 75% of BC transported into North America originated from Asia. Huang et al. (2012) simulated BC using the Sulfur Transport and Deposition Model (STEM), and found emissions outside North America contributed to 30–80% of column BC over North America in summer 2008. H. Wang et al. (2014) examined the long-term (1995-2005) average global source-receptor relationship of BC and found that BC emitted from the entire East Asia only contribute less than 5% to the total BC burden in North America, although the contribution is up to 40% near the west coast region. Few studies have examined the outflow from East Asia and inflow into North America contributed from source regions in and outside China. In addition, the emissions of BC from China increased dramatically during the last few years, with the annual total anthropogenic emissions estimated to have almost doubled in year 2014 compared to year 2000, shown in the newly developed Community Emissions Data System (CEDS; Hoesly et al. 2017). Therefore, the long-range transport of BC and source-receptor relationships could be quite different from previous studies.

Due to its warming effect in the climate system, BC is potentially important for climate mitigation and has drawn much attention recently. Source attribution of the direct radiative effect of BC is likely to be different from that of near-surface

concentration and column burden due to the dependence of radiative forcing on the vertical distribution of BC and its mixing state with other species that are influenced by different regional sources. In this study, we use the Community Earth System Model (CESM) with improved representations of aerosol transport and wet removal (H. Wang et al., 2013) and a BC source-tagging technique (H. Wang et al., 2014). Anthropogenic emissions from the newly developed CEDS inventory (Hoesly et al., 2017), as released for the Coupled Model Intercomparison Project Phase 6 (CMIP6), are used to examine the source attributions for mass concentration, long-range transport, and direct radiative forcing of BC in various regions of China. We aim to quantify: (1) source region contributions to concentrations of BC over various receptor regions in China; (2) contributions to changes in BC concentrations under polluted conditions; (3) source contributions to trans-boundary and trans-Pacific transport of BC; and (4) source contributions to direct radiative forcing of BC in China.

The CESM model, emissions, and numerical experiment are described in Section 2. Section 3 provides evaluation of the simulated concentration and aerosol absorption optical depth of BC in China. Section 4 investigates source contributions to near-surface concentrations, long-range transport and direct radiative forcing of BC over various receptor regions using the BC source-tagging technique in CESM. Section 5 summarizes these results.

2. Methods

We simulate the evolution and direct radiative forcing (DRF) of BC using CESM version 1.2 (Hurrell et al., 2013). The atmospheric model in CESM is version 5 of the Community Atmosphere Model (CAM5), with horizontal grid spacing of 1.9° latitude by 2.5° longitude and 30 vertical layers ranging from the surface to 3.6 hPa used in this study. The model treats the properties and processes of major aerosol species (sea salt, mineral dust, sulfate, black carbon, primary organic matter and secondary organic aerosol) using a three-mode modal aerosol module (MAM3), in which aerosol size distributions are represented by three lognormal modes: Aitken, accumulation, and coarse modes. BC is emitted to the accumulation mode. Mass mixing ratios of

different aerosol species and the number mixing ratio are predicted for each mode. A more detailed description of the MAM3 representation can be found in Liu et al. (2012). Aerosol dry deposition velocities are calculated using the Zhang et al. (2001) parameterization. The wet deposition of aerosols in our CAM5 model includes in-cloud wet removal (i.e., activation of interstitial aerosols to cloud-borne particles followed by precipitation scavenging) and below-cloud wet removal (i.e., capture of interstitial aerosol particles by falling precipitation particles) for both stratiform and convective clouds. Aerosol activation is calculated with the parameterization of Abdul-Razzak and Ghan (2000) for stratiform cloud throughout the column and convective cloud at cloud base, while the secondary activation above convective cloud base has a simpler treatment with an assumed maximum supersaturation in convective updrafts (H. Wang et al., 2013). The unified treatment for convective transport and aerosol wet removal along with the explicit aerosol activation above convective cloud base was developed by H. Wang et al. (2013) and included in the CAM5 version being used in this study. This implementation reduces the excessive BC aloft and better simulates observed BC concentrations in the mid- to upper-troposphere. Aerosol optical properties for each mode are parameterized according to Ghan and Zaveri (2007). Refractive indices for aerosols are taken from the OPAC (optical properties for aerosols and clouds) software package (Koepke and Schult, 1998), but for BC at solar wavelengths the values are updated from Bond and Bergstrom (2006). In MAM3, the aging process of BC is neglected by assuming the immediate mixing of BC with other aerosol species. Direct radiative forcing of BC is calculated as the difference in the top-of-the-atmosphere net radiative fluxes with and without BC for the all-sky condition following Ghan (2013).

Anthropogenic emissions used in this study are from the CEDS dataset, as released for the CMIP6 model experiments (Hoesly et al. 2017). This newly released emission inventory includes aerosol (black carbon, organic carbon) and aerosol precursor and reactive compounds (sulfur dioxide, nitrogen oxides, ammonia, carbon monoxide, and non-methane volatile organic compounds). The emissions are provided at monthly resolution for each year of 1750–2014 on a 0.5° x 0.5° grid and

include agricultural, energy, industry, residential, international shipping, solvents, surface transportation, waste treatment, and aircraft sectors. The biomass burning emissions used in this study are also developed for CMIP6 based on Global Fire Emission Database (GFED) version 4, Fire Model Intercomparison Project (FireMIP), visibility-observations and Global Charcoal Database (GCD) data (van Marle et al. 2016).

Figure 1a shows the horizontal spatial distribution of annual emissions of BC averaged over the most recent 5 years (2010–2014) and the seven geographical source regions tagged in continental China, including North China (NC), South China (SC), Southwest China (SW), Central-West China (CW), Northeast China (NE), Northwest China (NW), and Tibetan Plateau (TP). Figure 1b summarizes the total seasonal BC emissions in each of these source regions. North China has the largest annual emissions of BC in China, with maximum emission larger than 1.2 g C m^{-2} $year^{-1}$ and a regional total emission of 1089 Gg C $year^{-1}$ (44% of total emissions from continental China). Annual emissions of BC also have large values over South and Southwest China, with maximum values in the range of 0.8–1.2 g C m^{-2} $year^{-1}$, followed by Central-West and Northeast China. Over the less economically developed Northwest China and remote region Tibetan Plateau, emissions of BC are much lower than other regions in China. The seasonal mean emissions of BC also show the same spatial pattern as the annual means. BC had the largest emissions over North, South, and Southwest China in all seasons, among which emissions are strongest in December-January-February (DJF), especially over North China, resulting from domestic heating. The total seasonal emissions of BC in continental China are 797, 586, 537, and 577 Gg C in DJF, March-April-May (MAM), June-July-August (JJA), and September-October-November (SON), respectively, which add up to a total annual BC emissions of 2497 Gg C averaged over years 2010–2014. The anthropogenic emissions of BC in China in 2010–2014 are larger than those used in the previous studies for earlier years (Table S1), partly as a result of a higher estimate of BC emissions from coal coking production. The higher emissions likely lead to higher concentrations and direct radiative forcing, and source contributions of BC in

China, compared to the values reported in these studies. The DJF emissions account for 26–35% of annual total whereas emissions in JJA only account for 17–24% over the seven source regions in continental China. Total BC emissions from neighboring regions including rest of East Asia (REA, with China excluded), South Asia (SAS), Southeast Asia (SEA), and Russia/Belarussia/Ukraine (RBU) are shown in Figure 1c. These source regions outside China are consistent with source regions defined in the second phase of Hemispheric Transport of Air Pollution (HTAP2). South Asia and Southeast Asia have relatively high emissions. They may dominate the contribution to concentrations and direct radiative forcing of BC in China, especially southern and western China, from foreign sources through long-range transport.

An explicit BC source tagging capability was originally implemented in CAM5 by H. Wang et al. (2014), through which emissions of BC from independent source regions and/or sectors can be explicitly tracked. This method quantifies the source–receptor relationships of BC in any receptor region within a single model simulation without perturbing emissions from individual source regions or sectors. R. Zhang et al. (2015a,b) used this method to quantify the source attributions of BC in western North America, Himalayas, and Tibetan Plateau. The same BC source tagging technique is implemented to a newer model version (CAM5.3) and applied in this study to quantify the source attributions of concentration, transport and direct radiative forcing of BC in various regions of China. BC emissions (anthropogenic plus biomass burning) from seven geographical source regions, including North China, South China, Southwest China, Central-West China, Northeast China, Northwest China, Tibetan Plateau in China, and from rest of the world (RW) are tagged. Transport and physics tendencies are calculated separately for each tagged BC in the same way as the original BC simulation in CESM. We choose the seven individual regions (North China, South China, Southwest China, Central-West China, Northeast China, Northwest China, and Tibetan Plateau) and all seven regions combined (hereafter continental China) as receptor regions in this study to examine the source-receptor relationships of BC. While all emissions, including sulfur dioxides, organic carbon and BC, were used in the model simulation, tagging was only applied to BC emissions.

The CAM5 simulation is performed at 1.9° × 2.5° horizontal grid spacing using the specified-dynamics mode (Ma et al., 2013b), in which large-scale circulations (i.e., horizontal winds) are nudged to 6-hourly reanalysis data from the Modern Era Retrospective-Analysis for Research and Applications (MERRA) reanalysis data set (Rienecker et al., 2011) with a relaxation time scale of 6 hours (K. Zhang et al., 2014). The use of nudged winds allows for a more accurate simulation so that the key role of large-scale circulation patterns matches observations over the specified years. The simulation is run from year 2009 to 2014, with both time-varying aerosol emissions and meteorological fields. The first year is for spin-up and the last five years are used for analysis.

3. Model evaluation

The simulations of aerosols, especially BC, using CAM5 have been extensively evaluated against observations including aerosol mass and number concentrations, vertical profiles, aerosol optical properties, aerosol deposition, and cloud-nucleating properties in several previous studies (e.g., Liu et al., 2012, 2016; H. Wang et al., 2013; Ma et al., 2013b; Jiao et al., 2014; Qian et al., 2014; R. Zhang et al., 2015a,b). Here we focus on the evaluation of model performance in China using measurements of near-surface BC concentrations, vertical profiles, aerosol index derived from satellite, and aerosol absorption optical depth from the Aerosol Robotic Network (AERONET).

3.1 Mass concentrations and column burden of BC

Figure 2 presents spatial distributions of simulated seasonal mean near-surface concentrations and column burden of BC, both of which show a similar spatial pattern to emissions of BC (Figure 1a) with the largest values over North China and the lowest values over Northwest China and Tibetan Plateau. Near-surface model results are taken to be the lowest model layer (from surface to 985 hPa in average). Among all seasons, DJF has the highest BC levels, with values in the range of 6–12, 2–8, and 1–8 μg m^{-3} for near-surface concentrations and 6–12, 2–8, 1–12 mg m^{-2} for column burden over North, South, and Southwest China, respectively. In contrast, JJA has

281 the lowest BC concentrations over China due to the lower emissions and larger wet
282 scavenging associated with East Asian summer monsoon (Lou et al., 2016).
283 Averaged over continental China, near-surface BC concentrations are 2.5, 1.1, 0.8,
284 and 1.4 μg m^{-3} in DJF, MAM, JJA, and SON, respectively, with seasonal variability of
285 50%. The column burden of BC shows smaller seasonal variability (40%), with
286 area-weighted average of 2.5, 1.4, 1.0, and 1.4 mg m^{-2} in DJF, MAM, JJA, and SON,
287 respectively, in China. The magnitude, spatial distribution, and seasonal variations of
288 simulated near-surface BC concentrations over China are similar to those in Fu et al.
289 (2012) and X. Wang et al. (2013) using Intercontinental Chemical Transport
290 Experiment-Phase B (INTEX-B) emission inventory (Zhang et al., 2009) and those in
291 Li et al. (2016) using HTAP emission inventory (Janssens-Maenhout et al., 2015)
292 together with a global chemical transport model.
293 The simulated near-surface BC concentrations are evaluated here using
294 measurements at fourteen sites of the China Meteorological Administration
295 Atmosphere Watch Network (CAWNET) (Zhang et al., 2012). The locations of
296 CAWNET sites are shown in Figure S1a. The observational data include monthly BC
297 concentrations in years 2006–2007. Note that the simulated BC concentrations are
298 for years 2010–2014. Figure 3a compares the simulated seasonal mean near-surface
299 BC concentrations with those from CAWNET observations and Table S2 summarizes
300 the comparison in different regions, using modeled values from the grid cell
301 containing each observational site. Simulated BC concentrations at most sites are
302 within the range of one third to three times of observed values, except for Dunhuang
303 (94.68°E, 40.15°N) and Lhasa (91.13°E, 29.67°N) sites over western China, where
304 BC concentrations appear to be underestimated in the model (up to 20 times lower).
305 The possible bias is discussed in the following part. Over North China, simulated
306 concentrations are similar to observations in DJF, but underestimated in other
307 seasons. Over South China, the simulations do not have large biases compared to
308 the observed BC. However, simulated BC is underestimated in all seasons over
309 Southwest, Central-West, Northeast, Northwest China, and Tibetan Plateau.
310 Compared to the CAWNET data, the modeled near-surface BC concentrations have

311 a normalized mean bias (NMB) of –48%. Note that anthropogenic BC emissions went
312 up by a factor of 1.18 between 2006–2007 and 2010–2014. An emissions adjusted
313 comparison would result in an even larger underestimation. There are several
314 reasons that might cause low bias in this comparison. Liu et al. (2012) and H. Wang
315 et al. (2013) have previously found underestimation of BC concentrations over China
316 in CAM5 model and suggested the BC emissions may be significantly
317 underestimated. Using the global chemical transport model GEOS-Chem together
318 with emissions in 2006, Fu et al. (2012) found the simulated BC concentrations in
319 China were underestimated by 56%. With HTAP emissions at the year 2010 level, Li
320 et al. (2016) showed a low bias of 37% in simulated BC concentration in China.
321 Larger wet removal rate and shorter lifetime of aerosols along with the instantaneous
322 aging of BC in the MAM3 can also lead to the lower concentrations of BC (e.g., Wang
323 et al., 2011; Liu et al., 2012; H. Wang et al., 2013; Kristiansen et al., 2016).
324 Another potential cause for a bias in this comparison is spatial sampling bias.
325 Half of the CAWNET sites are located in urban areas, which will tend to have high
326 values near sources, whereas the modeled values represent averages over large grid
327 cells (R. Wang et al., 2014), as further discussed below.
328 The model captures well the spatial distribution and seasonal variation of BC
329 concentrations in China, having a statistically significant correlation coefficient of
330 +0.56 between simulated and observed seasonal BC concentrations over CAWNET
331 sites.
332 Figure S2 compares the observed and simulated vertical profiles of BC
333 concentrations in the East-Asian outflow region. The model successfully reproduces
334 the vertical profile of BC that was measured in March–April 2009 during the
335 A-FORCE field campaign and reported by Oshima et al. (2012).
336 **3.2 Aerosol absorption optical depth of BC**
337 To evaluate the simulated aerosol absorption optical depth (AAOD) of BC, the
338 AAOD data from AERONET (Holben et al., 2001) are used here. The locations of
339 AERONET sites in China are shown in Figure S1b. The observed AAOD are averaged
340 over years of 2010–2014 over seven sites and 2005–2010 over three sites with data

341 available. Most AERONET sites are over eastern and central China. AAOD of BC at
342 550nm are calculated by interpolating AAOD at 440 and 675 nm and removing AAOD
343 of dust from the retrieved AERONET AAOD following Bond et al. (2013). Figure 3b
344 compares the observed and simulated seasonal mean AAOD of BC at 550nm and
345 Table S3 summarizes the comparisons in different regions. The model has a low bias
346 in simulating AAOD of BC in China, smaller than the bias in near-surface
347 concentrations, with a NMB of –6%. As is the case with surface concentrations, this
348 bias could be due to model issues, such as BC transport or optical parameterization;
349 an underestimate in emissions; or spatial sampling bias. Simulated AAOD of BC are
350 within the range of one third to three times of observed values at most sites, with the
351 spatial distribution and seasonal variation broadly captured by the model. All but one
352 of the observations are located in the North and South China regions, and simulated
353 BC AAOD are, on average, similar to observations there. The AAOD from one
354 observation site in Central-West China is higher than the modeled value in DJF and
355 lower in other seasons. Note that, the observed AAOD of BC is derived from
356 AERONET measurements using the absorption Ångström exponent. A recent study
357 (Schuster et al., 2016) reported that absorption Ångström exponent is not a robust
358 parameter for separating out carbonaceous absorption in the AERONET database,
359 which could cause biases in the AAOD estimates.
360 Figure 4 shows the spatial distribution of simulated seasonal mean AAOD of total
361 aerosols and Aerosol Index (AI) derived from Ozone Monitoring Instrument (OMI)
362 measurements over years of 2010–2014. AI is a measure of absorbing aerosols
363 including BC and dust. Compared to satellite AI data, the model roughly reproduces
364 spatial distribution of total AAOD in China, with large values over North, South, and
365 Southwest China in all seasons. AI derived from Total Ozone Mapping Spectrometer
366 (TOMS) measurements (Figure S3) also shows similar pattern as simulated AAOD. It
367 should be noted that, besides BC, dust particles also largely contribute to AI and
368 produces large AI values over Northwest China.
369 To examine the potential model bias more broadly we compared the difference of
370 AAOD and AI between western and eastern China (Fig. 4). Averaging AI and AAOD

broadly over eastern and western China, we find that AAOD/AI is 0.055 over eastern China and 0.027 over western China. If we assume that the simulated AAOD do not have large biases over eastern China based on the evaluation against observations shown above (Fig. 3b and Table S3), then this difference hints a possible underestimation of BC column burden in the model over the western regions. However, it is difficult to draw a firm conclusion, given the likely differential role of dust in eastern vs western China. This differential likely also contributes to AAOD biases in modeling dust and may also impact biases in the satellite derived AI values.

4. Source contributions to BC concentrations, transport and direct radiative forcing

4.1. Source contributions to seasonal mean BC concentrations

Figure 5 shows the simulated spatial distribution of seasonal near-surface BC concentrations originating from the seven tagged source regions in continental China and all other sources from outside China (rest of the world, RW) and Table S4 summarizes these source-receptor relationships. It is not surprising that regional emissions largely influence BC concentrations in the same region. For example, emissions of BC from North China give 6.3 μg m^{-3} of BC concentrations over North China in DJF, whereas they only account for less than 1.8 μg m^{-3} over other regions in China. However, the relatively small amount of BC from upwind source regions can also be a large contributor to receptor regions near the strong sources. BC emissions from North China contribute large amount to concentrations over South, Southwest, Central-West, and Northeast China. BC emissions from South and Southwest China also produce a widespread impact on BC over other neighboring regions. The impacts of BC emitted from the remaining China regions are relatively small both in local and non-local regions due to weak emissions (Fig. 1b). All the sources in China have the largest impact in DJF, resulting from the strong BC emissions in winter, while emissions from outside China have the largest impact on BC over China in MAM due to the seasonal high emission over Southeast Asia and the strong springtime southwesterly winds.

401 Averaged over continental China, emissions of BC from North China produce
402 mean BC concentrations of 0.4–1.3 μg m^{-3}, followed by 0.2–0.5 μg m^{-3} from South
403 China and 0.1–0.3 μg m^{-3} from Southwest China emissions. For emissions over
404 Central-West China, Northeast China, Northwest China, and Tibetan Plateau, their
405 individual impact is less than 0.2 μg m^{-3}. In contrast, emissions from outside China
406 result in 0.12 μg m^{-3} of BC concentrations in China in MAM and less than 0.06 μg m^{-3}
407 in JJA and son. The simulated source contributions to column burden of BC are
408 shown in Figure S4. They present a very similar spatial distribution and seasonal
409 variation to those of near-surface BC concentrations. However, the emissions from
410 outside China have a larger impact on the average column burden of BC over China
411 than on surface concentrations, with a magnitude of 0.4 mg m^{-2} in MAM, which is
412 similar to that from sources in North China.
413 Figure 6 shows the spatial distribution of simulated relative contributions to
414 near-surface BC concentrations from sources in the seven regions in continental
415 China and those outside China by season. (The same plots for BC column burden are
416 shown in Figure S5.) For regions with higher emissions, their BC concentrations are
417 dominated by local emissions. In contrast, BC levels, especially column burden of BC,
418 over central and western China with lower emissions are strongly influenced by
419 non-local sources. Emissions from outside China can be the largest contributor to BC
420 over these regions. During DJF, MAM and SON, they contribute more than 70% to
421 both surface concentrations and column burden of BC in Tibetan Plateau, which is
422 important to the climate change due to the large climate efficacy of BC in snow (Qian
423 et al., 2011) and acceleration of snowmelt through elevated BC heat pump
424 mechanism (Lau et al., 2010). BC emissions from outside China also account for a
425 quite significant fraction of surface concentrations over Northwest and Southwest
426 China in MAM, which contribute to poor air quality over these regions.
427 Figure 7 summarizes source attribution for spatially averaged seasonal surface
428 BC concentrations for the seven receptor regions and continental China combined
429 (CN). Over North China, the majority of the BC concentrations are attributed to local
430 emissions in all seasons, with seasonal fractional contributions of 85–94%. Over

South China, the seasonal contributions from local emissions are in the range of 58–88%. Emissions from North China account for 35% of BC concentrations over South China in DJF, resulting from the wintertime northwesterly winds (Figure S6a), while emissions from outside China contribute about 10% in MAM due to the strong springtime biomass burning over southeast Asia and southwesterly winds transporting BC from southeast Asia to South China (Figure S6b). Southwest China has a similar level of local influence, with 47–81% of the BC concentration from local emissions, whereas 19% are due to emissions from outside China transported by westerly winds in MAM.

Non-local emissions from Southwest and North China together contribute 32–44% of BC concentration in Central-West China. North China emissions play an important role in BC concentrations over Northeast China, with relative contributions in a range of 21–30% in MAM, JJA and SON, while only 11% in DJF, which is associated with northwesterly winds in winter preventing northward transport of BC from North China to Northeast China. Over Northwest China and Tibetan Plateau, 18–34% and 46–78%, respectively, of BC originate from emissions outside China due to the low emissions over the less economically developed western China. For all of continental China as the receptor, the seasonal BC concentrations are largely attributed to the emissions from North and South China, with relative contributions ranging from 44–53% and 18–22%, respectively, followed by contributions from Southwest China (10–12%) and outside China (5–11%).

The source region contributions to column burden of BC in each receptor regions in China are shown in Figure S7. In general, impacts on the non-local BC column burden are larger than on surface concentrations because aerosol transport is relatively easier in free-troposphere than in the boundary layer (e.g., Yang et al., 2015). Column burdens of BC averaged over continental China mainly originate from emissions in North China, South China and outside China, with relative contributions ranging from 35–46%, 14–21% and 12–30%, respectively.

4.2. Source contributions during polluted days

Knowing the source attribution of BC during polluted days in China is important for policy makers, which could provide an effective way for the mitigation of poor air quality. Here, the polluted days are simply identified as days with daily concentrations of BC higher than 90th percentile of probability density function in each receptor regions. A total of different 45 days in winter in the 5-year simulation are identified as polluted days for each region in China.

Figure 8 shows the DJF composite differences in near-surface BC concentrations and winds at 850 hPa between polluted and normal days for each receptor region, and Figure 9 summarizes the local and non-local source contributions to the differences. When North China is under the polluted condition, BC concentrations are higher by more than 70% compared to DJF average over North China, with a maximum increase exceeding 5 μg m^{-3}. North China local emissions contribute 5.6 μg m^{-3} to the averaged increase in BC concentrations over North China during North China polluted days, about 90% of the total increase. In winter, eastern China is dominated by strong northwesterly winds (Figure S6a). The anomalous southerly winds during polluted days (relative to DJF average) over North China prevent the high BC concentrations from being transported to South China, leading to a reduced ventilation and accumulated aerosols in North China.

Over South China, BC concentrations increase by up to 2–5 μg m^{-3}, in part due to the transport from North China by anomalous northerly winds in the north part of South China in South China polluted days. On average, contribution of North China emissions to mean concentrations over South China increases by 2.0 μg m^{-3} (60% of total increase) during the South China polluted days.

During polluted days in Southwest China, the anomalous northeasterly winds in the east part of Southwest China bring in BC from the highly polluted eastern China, resulting in 2.1 μg m^{-3} increase (74% of total increase) in the Southwest China, which is much larger than the 0.7 μg m^{-3} contribution from the Southwest China local emissions.

The increase in BC concentrations during polluted days over Central-West China is also largely influenced by the accumulation effect of the anomalous winds over

eastern and central China, which also transport BC from Southwest and eastern China into the receptor region.

The polluted days in Northeast China are caused by both the accumulation of local emissions due to the reduced prevailing northeasterly winds and anomalous transport of BC from North China.

Emissions from outside China could contribute to increases in BC concentrations over Northwest China and Tibetan Plateau during polluted days. However, during wintertime regional polluted days in eastern and central China, the contributions of emissions from outside China do not have a significant influence on the changes in BC concentrations.

These results suggest that the transport of aerosols plays an important role in increasing BC concentrations during regional polluted days in eastern and central China. Reductions in local emissions could benefit mitigation of both local and non-local haze in China. Emissions from outside China are not as important to hazy pollution in eastern and central China, where haze episodes occur frequently in winter due to relatively high anthropogenic aerosol emissions and abnormal meteorological conditions (Sun et al., 2014; R. H. Zhang et al., 2014; Yang et al., 2016). Note that, in this study, we only focus on the source-receptor relationships related to the wind anomalies during polluted days. In addition to winds, changes in other meteorological fields, such as precipitation, temperature, humidity, and planetary boundary layer height, could also influence the contributions of local aerosols between polluted and normal days. Although the BC emissions used in the simulation include a seasonal variability that could cause some variations in simulated concentrations, the monthly variability in DJF of BC emissions is less than 4% over China, which is negligible compared to the differences in concentrations between polluted and normal days.

4.3. Source contributions to trans-boundary and trans-Pacific transport

Considering the large contributions of emissions from South and Southeast Asia to MAM BC concentrations in the southwest China (Figure 6) and the large outflow of aerosols from East Asia in springtime (Yu et al., 2008), it is valuable to examine the

521 inflow and outflow of BC in China. Figures S8a and S8b show the vertical distribution
522 of source contributions of emissions from outside China to BC concentrations
523 averaged over 75°–120°E and 25°–35°N, respectively, around the south boundary of
524 continental China in MAM. High concentrations of BC originating from South and
525 Southeast Asia are lifted to the free atmosphere in the south slope of Tibetan Plateau.
526 Then westerly winds transport these BC particles to Southwest China and South
527 China in both low- and mid-troposphere. Figures S8c and S8d present the
528 contributions of emissions from China to BC concentrations averaged over 120°–
529 135°E and 20°–50°N, respectively, around the east boundary of continental China. In
530 MAM, the northward meridional winds over 25°–35°N and the southward meridional
531 winds over 40°–50°N lead to the accumulation of BC in the lower atmosphere in
532 eastern China. Westerly winds then transport these BC out of China mostly under 500
533 hPa.
534 Figure 10 shows the spatial distribution of column burden and surface
535 concentrations of BC resulting from emissions in and outside China in MAM. Column
536 burden is used to represent the outflow in this study following previous studies (Chin et
537 al., 2007; Hadley et al., 2007). There are strong outflows across the Pacific Ocean
538 originating from emissions both in and outside China. Emissions from China contribute
539 0.20 mg m^{-2} (or 55%) of MAM mean BC along 150°E averaged over 20°–60°N,
540 whereas emissions outside China contribute 0.16 mg m^{-2} (or 45%). It suggests that
541 both emissions from China and outside China are important for the outflow from East
542 Asia. The yearly contribution from emissions from China to outflow from East Asia in
543 this study is 59%, similar to the contribution of 61% in Matsui et al. (2013) calculated
544 based on eastward BC mass flux using WRF-CMAQ model with INTEX-B missions.
545 Averaged over western United States (125°–105°W, 30°–50°N), emissions from
546 China account for 8% of near-surface BC concentrations and 29% in column burden in
547 MAM, indicating that emissions from China could have a significant impact on air
548 quality in western United States. More than half of the China contribution to BC over
549 western United States originates from eastern China (i.e., the tagged North and South
550 China).

551

552 **4.4. Source contributions to direct radiative forcing**

553 The high concentrations of BC in China could also have a significant impact on the
554 climate system through atmospheric heating or direct radiative forcing. As shown in
555 Figure 11, the annual mean direct radiative forcing (DRF) of BC at TOA is as high as
556 3–5 W m^{-2} at some locations. Similar to the source attributions of BC concentrations
557 (Figure 5) and burden (Figure S4), regional sources contribute the largest to DRF over
558 the respective local regions. Among all the source regions in China, emissions from
559 North, South, and Southwest China contribute the largest to local DRF of BC, with
560 maximum DRF in a range of 3–5, 2–3, and 3–5 W m^{-2}, respectively. Other sources
561 regions in China have relatively low contributions, with maximum values less than 2 W
562 m^{-2}. Emissions outside China lead to 1–2 W m^{-2} of DRF of BC over South, Southwest,
563 Northwest China and Tibetan Plateau, and 0.2–1 W m^{-2} over other parts of China, an
564 effect that is quite widespread.

565 The total DRF of BC averaged over continental China simulated in this study is
566 2.20 W m^{-2}, larger than 0.64–1.55 W m^{-2} in previous studies (Wu et al., 2008; Zhuang
567 et al., 2011; Li et al., 2016), probably due to the different emissions in the time periods
568 of study, as shown in Table S5. Emissions outside China have the largest
569 contributions to DRF of BC in China compared to any of the individual source regions
570 in China, with an averaged contribution of 0.78 W m^{-2} (35%). This fractional
571 contribution from emissions outside China is larger than 25% in Li et al. (2016),
572 however we use different emissions, model and meteorology. Emissions from North
573 China result in 0.55 W m^{-2} (25%) of DRF of BC over China, followed by 0.30 W m^{-2}
574 (14%) and 0.28 W m^{-2} (13%) from Southwest and South China, respectively.
575 Emissions from Central-West, Northeast, Northwest China, and Tibetan Plateau taken
576 together account for 0.29 W m^{-2} (13%) of DRF of BC over China.

577 Figure 12a shows the seasonal mean DRF of BC averaged over China as a
578 function of regional BC emissions. Because of high emissions, DRF of BC emitted
579 from North China is the largest in all seasons, with values in a range of 0.5–0.8 W m^{-2}
580 averaged over China, followed by 0.2–0.5 W m^{-2} from South and Southwest China. BC

581 from the other tagged regions in China contribute less than 0.2 W m^{-2} in all seasons. In
582 general, BC DRF in each season is proportional to its emission rate.
583 Figure 12b presents the seasonal DRF efficiency of BC emitted from the tagged
584 regions and Table S6 summarizes these efficiencies. The variability of DRF efficiency
585 for forcing over China is determined by several factors, such as incoming solar
586 radiation (location of source regions), BC column burden and vertical distribution, and
587 transport out of the region. The China DRF efficiency is largest in western China (NW
588 and TP). This spatial pattern was also found by Henze et al. (2012). It can be
589 explained by the increase of multiple scattering effects and attenuation of the
590 transmitted radiation for large AOD (García et al., 2012). The Northeast China region
591 has a low China DRF efficiency due to transport eastward outside of China. The
592 remaining central and southern China regions have China DRF efficiencies that are
593 fairly consistent, varying by 20-30% about the average. The annual mean and
594 regional mean DRF efficiency in China is 0.88 W m^{-2} Tg^{-1}, within the range of 0.41–
595 1.55 W m^{-2} Tg^{-1} from the previous studies (Table S5).
596 DRF efficiencies of BC from most regions have higher values in JJA and lower
597 values in DJF. This is primarily due to more incoming solar radiation in summer.
598 Insolation is the largest over Northwest China in JJA, together with less precipitation
599 than other regions, resulting in large DRF efficiency there. Global BC DRF efficiency,
600 particularly the annual average, is fairly similar for central, southern, and eastern
601 China regions (Fig. 12c, d). Global efficiency is still much higher for the western
602 regions.
603 BC emission reductions may impact mitigation of climate change and improve air
604 quality. To compare the relative importance of climate and air quality effects of BC
605 from different regions in China, Fig. 13 shows the near-surface concentration and
606 column burden efficiency of BC over China and globally and Table S7 summarizes
607 these efficiencies. For near-surface concentration (Fig. 13a and 13b), the efficiencies
608 are largest in DJF and lowest in JJA, in contrast to the DRF efficiencies, resulting
609 from the less precipitation and wet deposition of aerosols in winter. Unlike the DRF
610 efficiencies, the near-surface concentration efficiencies over eastern China are

similar and even larger than those for central and western China. These results suggest that reduction in BC emissions in eastern China could benefit more on the regional air quality in China, especially in winter haze season.

The relative distributions of column burden efficiencies (Fig. 13c and 13d) are similar to the DRF efficiencies for the major emitting region in China, indicating that aerosol lifetime in atmosphere drives DRF that influences regional and global climate. The western regions (NW and TP), as expected, have a higher forcing per unit column burden.

5. Conclusions and discussions

In this study, the Community Earth System Model (CESM) with a source-tagging technique is used to quantify the contributions of BC emitted from seven regions in continental China, including North China (NC), South China (SC), Southwest China (SW), Central-West China (CW), Northeast China (NE), Northwest China (NW), and Tibetan Plateau (TP), and sources outside China (RW) to concentrations, haze formation, trans-boundary and trans-Pacific transport, and direct radiative forcing (DRF) of BC in China. The anthropogenic emissions of BC for years 2010-2014 used in this study were developed for the Coupled Model Intercomparison Project Phase 6 (CMIP6) from the Community Emissions Data System (CEDS). The annual total emission of BC from continental China is 2497 Gg C averaged over years 2010–2014. The model captures well the spatial distribution and seasonal variation in China. AAOD compares well with measurements, which are largely located in central and eastern China. Surface BC concentrations are underestimated by 48% compared to point observations.

The individual source regions are the largest contributors to their local BC concentration levels. Over North China where the air quality is often poor, about 90% of near-surface BC concentration is contributed by local emissions. However, some source regions also impact BC in neighboring regions. Due to the seasonal variability of winds and emission rates, emissions from North China account for 35% of near-surface BC concentrations over South China in DJF

641 (December-January-February), while emissions from outside China contribute about
642 10% in MAM (March-April-May). Over Southwest China, 19% of BC in MAM comes
643 from sources outside China. Southwest and North China emissions contribute largely
644 to BC in Central-West China. North China emissions have a contribution in a range of
645 21–30% to BC concentrations in Northeast China. Over Northwest China and Tibetan
646 Plateau, more than 20% and 40% of BC, respectively, originates from emissions
647 outside China. These indicate that, for regions with high emissions, their BC
648 concentrations are dominated by local emissions. In contrast, BC levels over central
649 and western China with lower emissions are more strongly influenced by non-local
650 emissions. For all continental China as a whole, seasonal BC concentrations are
651 largely due to emissions from North and South China, with relative contributions
652 ranging from 44–53% and 18–22%, respectively, followed by contributions from
653 Southwest (10–12%) and outside China (5–11%).

654 Emissions from non-local sources together with abnormal winds are one of the
655 important factors contributing to high winter time pollution events in China. Over
656 South China, about 60% of the increase in BC concentrations during high pollution
657 conditions results from North China emissions. The increases in BC concentrations
658 during polluted days over Southwest, Central-West and Northeast China are strongly
659 influenced by emissions from eastern China. Emissions from outside China could
660 contribute significantly to increases in BC concentrations over Northwest China and
661 Tibetan Plateau during their polluted days. However, emissions from outside China do
662 not have a significant contribution to haze in eastern and central China, suggesting
663 that reduction in emissions within China would be needed to mitigate both local and
664 non-local BC concentrations under high-polluted conditions.

665 Emissions from regions in and outside China both account for about half of BC
666 outflow from East Asia, suggesting that emissions from China and other regions are
667 equally important for the BC outflow from East Asia. Through long-range transport,
668 emissions from China result in 8% of near-surface BC concentration and 29% in
669 column burden over western United States in MAM, indicating that emissions from
670 China could have an impact on air quality in western United States.

671 The total DRF of BC averaged over continental China simulated in this study is
672 2.20 W m^{-2}. Among the tagged regions, emissions outside China have the largest
673 single contribution to DRF of BC in China, with an average contribution of 35%,
674 followed by 25%, 14%, and 13% due to emissions from North, South and Southwest
675 China, respectively. DRF efficiencies over eastern China are small compared to
676 central and western China in all seasons. For near-surface concentration, the
677 efficiencies are largest in DJF and lowest in JJA, and efficiencies over eastern China
678 are similar and even larger than central and western China. These suggest that
679 reduction in BC emissions over eastern China could benefit more on the regional air
680 quality in China, especially in winter haze season.
681 Note that the model largely underestimates BC concentrations over China,
682 compared to the observation, which has also been reported in many previous studies
683 using different models and different emission inventories (e.g., Liu et al., 2012; Fu et
684 al., 2012; Huang et al., 2013; H. Wang et al., 2013; Q. Wang et al., 2014; R. Wang et
685 al., 2014; Li et al., 2016). One possible reason is that in situ measurements are point
686 observations, while the model does not treat the subgrid variability of aerosols and
687 assumes aerosols are uniformly distributed over the grid cell. R. Wang et al. (2014)
688 found a reduction of negative bias (from −88% to −35%) in the modeled surface BC
689 concentrations when using high-resolution emissions and modeling at 0.5° X 0.7°
690 resolution. This result indicates that the siting of observational stations can result in
691 an artificial bias when comparing with relatively coarse model results. Further
692 investigation of this siting/resolution bias is warranted, including investigation on
693 whether this type of bias might extend, presumably to a lesser extent, also to AAOD
694 measurements.
695 Further reasons that could contribute to this bias are emission underestimation or
696 inaccurate aerosol processes in the model. Given that the differences between
697 modeled and observed AAOD over eastern China are relatively small (–6%), we
698 conclude that, given current evidence, the total amount of atmospheric BC in these
699 simulations is reasonable at least in this sub-region.

Over eastern China, the BC concentrations are dominated by local emissions in this study, with local contribution of 58–94%. The underestimation of simulated BC concentrations over eastern China is more likely due to either underestimation of local emissions, too much aerosol removal within these regions, or resolution bias between observations and model grids. Over western China, 18–78% of the BC originates from emissions outside China. Thus biases of simulated BC concentrations could also come from underestimation of emissions outside China and or too much removal of BC during long-range transport. Satellite data are a promising method to validate modeling and emissions inventories, given that they do not depend on the location of observing stations, providing more uniform spatial coverage. A comparison of modeled AAOD and satellite AI provides an indication that the modeled burden in western China is underestimated, although the role of dust needs to be better characterized.

Uncertainty in China BC emissions has been estimated as –43% to 93% by Lu et al. (2011), –50% to 164% by Qin and Xie (2012), ±176% by Kurokawa et al. (2013), and –28 to 126% by Zhao et al. (2013). The BC emissions estimates used here for China in 2010 are 40% higher than those of Zhao et al. (2013) and Lu et al. (2011) and 30% higher than Klimont et al. (2016), in large part due to a higher estimate of BC emissions from coal coke production. Emissions from coke production are particularly uncertain given that “there are no measurements for $PM_{2.5}$ and BC emissions” (Huo et al. 2012) available to guide inventory estimates. Total rest of the world emissions other than China, which appear to be a major contributor to burdens over western regions, are within 1% of those from Klimont et al. (2016).

BC aging in the atmosphere is important for BC concentration and its optical properties, which transforms BC from hydrophobic aggregates to hydrophilic particles coated with soluble materials (Cheng et al., 2006). He et al. (2015, 2016a) found that BC optical properties varied by a factor of two or more due to different coating structures during BC aging process based on their theoretical and experimental intercomparison. Oshima et al. (2009) and He et al. (2016b) pointed out that the use of various microphysical BC aging schemes could significantly improve simulations of

730 BC concentrations, compared to the simplified aging parameterizations. Liu et al.
731 (2012) also reported that the wet removal rate of BC simulated in standard CAM5 is 60%
732 higher than AeroCom multi-model mean due to the rapid or instantaneous aging of BC.
733 H. Wang et al. (2013) showed that the explicit treatment of BC aging process with slow
734 aging assumptions in CAM5 could significantly increase BC lifetime and the efficiency
735 of BC long-range transport. In the three-mode aerosol module (MAM3) of CAM5 used
736 in this study, the aging process of BC is neglected by assuming the immediate internal
737 mixing of BC with other aerosol species in the same mode. This assumption could
738 lead to an overestimation of wet removal of BC and, therefore, an underestimation of
739 BC concentrations, absorption optical depth (Fig. 3) and direct radiative forcing. In
740 addition, the internally-mixed optical treatment in CAM5 could also cause bias in BC
741 absorption calculation. However, H. Wang et al. (2014) examined source-receptor
742 relationships for BC under the different BC aging assumptions and found that the
743 quantitative source attributions varied slightly while the qualitative source-receptor
744 relationships still hold. Therefore, although the magnitude of simulated BC and its
745 optical properties could be underestimated due to the instantaneous aging of BC and
746 uncertainty in coating structures, we expect that the aging treatment in MAM3 of
747 CAM5 should not influence the qualitative source attributions examined in this study.
748 In this study, BC is used as an indicator of pollution (or air quality) in China.
749 Although BC is often co-emitted with other species, such as primary organic matter,
750 organic gases and sulfuric gases, source-receptor relationship of BC may not fully
751 represent that of total aerosols. The contribution of BC to total near-surface $PM_{2.5}$
752 concentrations averaged over China is less than 10%. Other aerosols, such as sulfate,
753 are dominant in China during polluted days. The spatio-temporal variations and
754 source contributions of these species are largely different from those of BC because
755 spatial distributions of emissions (e.g., SO_2) and formation processes can be
756 considerably different. For example, Matsui et al. (2009) showed that primary aerosols
757 around Beijing were determined by emissions within 100 km around Beijing within the
758 preceding 24 hours, while emissions as far as 500 km and within the preceding 3 days
759 were found to affect secondary aerosols in Beijing. Thus, the secondary aerosols

could have larger contributions from non-local emissions than BC. BC concentrations are highest in winter over China due to higher emissions, while sulfate concentrations reach maximum in summer when the strong sunlight and high temperature favor the sulfate formation. Therefore, knowing the accurate source attributions of air pollution in China requires source tagging for more aerosol species, such as sulfate.

Acknowledgments.

This research was supported by the National Atmospheric and Space Administration's Atmospheric Composition: Modeling and Analysis Program (ACMAP), award NNH15AZ64I. We also acknowledge additional support from the U.S. Department of Energy (DOE), Office of Science, Biological and Environmental Research. The Pacific Northwest National Laboratory is operated for DOE by Battelle Memorial Institute under contract DE-AC05-76RLO1830. The CESM project was supported by the National Science Foundation and the DOE Office of Science. The satellite-derived Total Ozone Mapping Spectromenter Aerosol Index monthly data sets are obtained from the Web site at http://disc.sci.gsfc.nasa.gov/data-holdings/PIP/aerosol_index.shtml. The National Energy Research Scientific Computing Center (NERSC) provided computational resources. Model results are available through NERSC upon request.

References

Abdul-Razzak, H., and Ghan, S. J.: A parameterization of aerosol activation: 2. Multiple aerosol types, J. Geophys. Res., 105, 6837–6844, doi:10.1029/1999JD901161, 2000.

Anenberg, S. C., Talgo, K., Arunachalam, S., Dolwick, P., Jang, C., and West, J. J.: Impacts of global, regional, and sectoral black carbon emission reductions on surface air quality and human mortality, Atmos. Chem. Phys., 11, 7253-7267, doi:10.5194/acp-11-7253-2011, 2011.

Bond, T. C., Streets, D. G., Yarber, K. F., Nelson, S. M., Woo, J.-H., and Klimont, Z.: A technology-based global inventory of black and organic carbon emissions from combustion, J. Geophys. Res., 109, D14203, doi:10.1029/2003JD003697, 2004.

Bond, T. C., and Bergstrom, R. W.: Light absorption by carbonaceous particles: An investigative review, Aerosol. Sci. Technol., 40, 27–67, doi:10.1080/02786820500421521, 2006.

Bond, T. C., Bhardwaj, E., Dong, R., Jogani, R., Jung, S., Roden, C., Streets, D. G., and Trautmann, N. M.: Historical emissions of black and organic carbon aerosol from energy-related combustion, 1850–2000, Global Biogeochem. Cycles, 21, GB2018, doi:10.1029/2006GB002840, 2007.

803 Bond, T. C., Doherty, S. J., Fahey, D. W., Forster, P. M., Berntsen, T., DeAngelo,B.
804 J., Flanner, M. G., Ghan, S., Kärcher, B., Koch, D., Kinne, S., Kondo, Y., Quinn,
805 P. K., Sarofim, M. C., Schultz, M. G., Schulz, M., Venkataraman, C., Zhang, H.,
806 Zhang, S., Bellouin, N., Guttikunda, S. K., Hopke, P. K., Jacob- son, M. Z.,
807 Kaiser, J. W., Klimont, Z., Lohmann, U., Schwarz, J. P., Shindell, D., Storelvmo,
808 T., Warren, S. G., and Zender, C. S.: Bounding the role of black carbon in the
809 climate sys- tem: A scientific assessment, J. Geophys. Res., 118, 5380–5552,
810 doi:10.1002/jgrd.50171, 2013.
811
812 Cheng, Y. F., Eichler, H., Wiedensohler, A., Heintzenberg, J., Zhang, Y. H., Hu, M.,
813 Herrmann, H., Zeng, L. M., Liu, S., Gnauk, T., Bruggemann, E., and He, L. Y.:
814 Mixing state of el- emental carbon and non-light-absorbing aerosol components
815 de- rived from in situ particle optical properties at Xinken in Pearl River Delta of
816 China, J. Geophys. Res. Atmos., 111, D20204, doi:10.1029/2005JD006929,
817 2006.
818
819 Chin, M., Diehl, T., Ginoux, P., and Malm, W.: Intercontinental transport of pollution
820 and dust aerosols: implications for regional air quality, Atmos. Chem. Phys., 7,
821 5501-5517, doi:10.5194/acp-7-5501-2007, 2007.
822

823 Ding, Y. H., and Liu, Y. J.: Analysis of long-term variations of fog and haze in China in
824 recent 50 years and their relations with atmospheric humidity, Sci. China Earth
825 Sci., 57, 36–46, doi:10.1007/s11430-013-4792-1, 2014.
826
827 Flanner, M. G., Zender, C. S., Randerson, J. T., and Rasch, P. J.: Present day
828 climate forcing and response from black carbon in snow, J. Geophys. Res., 112,
829 D11202, doi:10.1029/2006JD008003, 2007.
830
831 Fu, T.-M., Cao, J. J., Zhang, X. Y., Lee, S. C., Zhang, Q., Han, Y. M., Qu, W. J., Han,
832 Z., Zhang, R., Wang, Y. X., Chen, D., and Henze, D. K.: Carbonaceous aerosols
833 in China: top-down constraints on primary sources and estimation of secondary
834 contribution, Atmos. Chem. Phys., 12, 2725-2746,
835 doi:10.5194/acp-12-2725-2012, 2012.
836
837 García, O. E., Díaz, J. P., Expósito, F. J., Díaz, A. M., Dubovik, O., Derimian, Y.,
838 Dubuisson, P., and Roger, J.-C.: Shortwave radiative forcing and efficiency of key
839 aerosol types using AERONET data, Atmos. Chem. Phys., 12, 5129-5145,
840 doi:10.5194/acp-12-5129-2012, 2012.
841
842 Ghan, S. J., and Zaveri, R. A.: Parameterization of optical properties for hydrated
843 internally mixed aerosol, J. Geophys. Res., 112, D10201,
844 doi:10.1029/2006JD007927, 2007.

Ghan, S. J., Technical Note: Estimating aerosol effects on cloud radiative forcing, Atmos. Chem. Phys., 13, 9971-9974, doi:10.5194/acp-13-9971-2013, 2013.

Hadley, O. L., Ramanathan, V., Carmichael, G. R., Tang, Y., Corrigan, C. E., Roberts, G. C., and Mauger, G. S.: Trans-Pacific transport of black carbon and fine aerosols (D < 2.5 μm) into North America, J. Geophys. Res., 112, D05309, doi:10.1029/2006JD007632, 2007.

He, C., Liou, K.-N., Takano, Y., Zhang, R., Levy Zamora, M., Yang, P., Li, Q., and Leung, L. R.: Variation of the radiative properties during black carbon aging: theoretical and experimental intercomparison, Atmos. Chem. Phys., 15, 11967-11980, doi:10.5194/acp-15-11967-2015, 2015.

He, C., Takano, Y., Liou, K.-N., Yang, P., Li, Q., and Mackowski, D. W.: Intercomparison of the GOS approach, superposition T- matrix method, and laboratory measurements for black carbon optical properties during aging, J. Quant. Spectrosc. Ra., 184, 287–296, doi:10.1016/j.jqsrt.2016.08.004, 2016a.

He, C., Li, Q., Liou, K.-N., Qi, L., Tao, S., and Schwarz, J. P.: Microphysics-based black carbon aging in a global CTM: constraints from HIPPO observations and

implications for global black carbon budget, Atmos. Chem. Phys., 16, 3077-3098, doi:10.5194/acp-16-3077-2016, 2016b.

Henze, D. K., Shindell, D. T., Akhtar, F., R. Spurr, J. D., Pinder, R. W., Loughlin, D., Kopacz, M., Singh, K., and Shim, C.: Spatially refined aerosol direct radiative forcing efficiencies, Environ. Sci. Technol., 46, 9511–9518, doi:10.1021/es301993s, 2012.

Holben, B. N., Tanré, D., Smirnov, A., Eck, T. F., Slutsker, I., Abuhassan, N., Newcomb, W. W., Schafer, J. S., Chatenet, B., Lavenu, F., Kaufman, Y. J., Castle, J. V., Setzer, A., Markham, B., Frouin, D. C. R., Halthore, R., Karneli, A., O'Neill, N. T., Pietras, C., Pinker, R. T., Voss, K., and Zibordi, G.: An emerging ground-based aerosol climatology: Aerosol optical depth from AERONET, J. Geophys. Res., 106, 12 067–12 098, 2001.

Huang, Y., Wu, S., Dubey, M. K., and French, N. H. F.: Impact of aging mechanism on model simulated carbonaceous aerosols, Atmos. Chem. Phys., 13, 6329-6343, doi:10.5194/acp-13-6329-2013, 2013.

Huo, H., Lei, Y., Zhang, Q., Zhao, L. J., and He, K. B.: China's coke industry: Recent policies, technology shift, and implication for energy and the environment, Energ. Policy., 51, 397–404, doi:10.1016/j.enpol.2012.08.041, 2012.

888

889 Hurrell, J. W., Holland, M. M., Gent, P. R., Ghan, S., Kay, J. E., Kushner, P. J.,
890 Lamarque, J. F., Large, W. G., Lawrence, D., Lind- say, K., Lipscomb, W. H.,
891 Long, M. C., Mahowald, N., Marsh, D. R., Neale, R. B., Rasch, P., Vavrus, S.,
892 Vertenstein, M., Bader, D., Collins, W. D., Hack, J. J., Kiehl, J., and Marshall, S.:
893 The Community Earth System Model A Framework for Collabora- tive Research,
894 B. Am. Meteorol. Soc., 94, 1339–1360, 2013.

895

896 IPCC, 2013, Climate Change 2013: the Physical Science Basis. Contribution of
897 Working Group I to the Fifth Assessment Report of the Intergovernmental Panel
898 on Climate Change. Cambridge University Press, Cambridge, United Kingdom
899 and New York, NY, USA, p. 1535.

900

901 Jacobson, M. Z.: Effects of externally-through-internally-mixed soot inclusions within
902 clouds and precipitation on global climate, J. Phys. Chem. A, 110, 6860–6873,
903 doi:10.1021/Jp056391r, 2006.

904

905 Janssen, N. A. H., Gerlofs-Nijiland, M. E., Lanki, T., Salonen, R. O., Cassee, F.,
906 Hoek, G., Fischer, P., Brunekreef, B., and Krzyzanowski, M.: Health Effects of
907 Black Carbon, World Health Organization, Copenhagen, 2012.

908

Janssens-Maenhout, G., Crippa, M., Guizzardi, D., Dentener, F., Muntean, M., Pouliot, G., Keating, T., Zhang, Q., Kurokawa, J., Wankmüller, R., Denier van der Gon, H., Kuenen, J. J. P., Klimont, Z., Frost, G., Darras, S., Koffi, B., and Li, M.: HTAP_v2.2: a mosaic of regional and global emission grid maps for 2008 and 2010 to study hemispheric transport of air pollution, Atmos. Chem. Phys., 15, 11411-11432, doi:10.5194/acp-15-11411-2015, 2015.

Jiao, C., Flanner, M. G., Balkanski, Y., Bauer, S. E., Bellouin, N., Berntsen, T. K., Bian, H., Carslaw, K. S., Chin, M., De Luca, N., Diehl, T., Ghan, S. J., Iversen, T., Kirkevåg, A., Koch, D., Liu, X., Mann, G. W., Penner, J. E., Pitari, G., Schulz, M., Seland, Ø., Skeie, R. B., Steenrod, S. D., Stier, P., Takemura, T., Tsigaridis, K., van Noije, T., Yun, Y., and Zhang, K.: An AeroCom assessment of black carbon in Arctic snow and sea ice, Atmos. Chem. Phys., 14, 2399-2417, doi:10.5194/acp-14-2399-2014, 2014.

Klimont, Z., Kupiainen, K., Heyes, C., Purohit, P., Cofala, J., Rafaj, P., Borken-Kleefeld, J., and Schöpp, W.: Global anthropogenic emissions of particulate matter including black carbon, Atmos. Chem. Phys. Discuss., doi:10.5194/acp-2016-880, in review, 2016.

929 Koepke, M. H. P., and Schult, I.: Optical properties of aerosols and clouds: The
930 software package opac, Bull. Am. Meteorol. Soc., 79, 831–844,
931 doi:10.1175/1520-0477(1998)079<0831:OPOAAC>2.0.CO;2, 1998.
932
933 Kristiansen, N. I., Stohl, A., Olivié, D. J. L., Croft, B., Søvde, O. A., Klein, H.,
934 Christoudias, T., Kunkel, D., Leadbetter, S. J., Lee, Y. H., Zhang, K., Tsigaridis,
935 K., Bergman, T., Evangeliou, N., Wang, H., Ma, P.-L., Easter, R. C., Rasch, P. J.,
936 Liu, X., Pitari, G., Di Genova, G., Zhao, S. Y., Balkanski, Y., Bauer, S. E.,
937 Faluvegi, G. S., Kokkola, H., Martin, R. V., Pierce, J. R., Schulz, M., Shindell, D.,
938 Tost, H., and Zhang, H.: Evaluation of observed and modelled aerosol lifetimes
939 using radioactive tracers of opportunity and an ensemble of 19 global models,
940 Atmos. Chem. Phys., 16, 3525-3561, doi:10.5194/acp-16-3525-2016, 2016.
941
942 Kurokawa, J., Ohara, T., Morikawa, T., Hanayama, S., Janssens-Maenhout, G.,
943 Fukui, T., Kawashima, K., and Akimoto, H.: Emissions of air pollutants and
944 greenhouse gases over Asian regions during 2000–2008: Regional Emission
945 inventory in ASia (REAS) version 2, Atmos. Chem. Phys., 13, 11019-11058,
946 doi:10.5194/acp-13-11019-2013, 2013.
947
948 Lau, K.-M., Kim, M. K., Kim, K.-M., and Lee, W. S.: Enhanced surface warming and
949 accelerated snow melt in the Himalayas and Tibetan Plateau induced by

absorbing aerosols, Environ. Res. Lett., 5, 025204, doi:10.1088/1748-9326/5/2/025204, 2010.

Li, K., Liao, H., Mao, Y. H., and Ridley, D. A.: Source sector and region contributions to concentration and direct radiative forcing of black carbon in China, Atmos. Environ., 124, 351–366, doi:10.1016/j.atmosenv.2015.06.014, 2016.

Liao, H., Chang, W. Y., and Yang, Y.: Climatic effects of air pollutants over China: A review, Adv. Atmos. Sci., 32, 115–139, doi:10.1007/s00376-014-0013-x, 2015.

Liu, X., Easter, R. C., Ghan, S. J., Zaveri, R., Rasch, P., Shi, X., Lamarque, J.-F., Gettelman, A., Morrison, H., Vitt, F., Conley, A., Park, S., Neale, R., Hannay, C., Ekman, A. M. L., Hess, P., Mahowald, N., Collins, W., Iacono, M. J., Bretherton, C. S., Flanner, M. G., and Mitchell, D.: Toward a minimal representation of aerosols in climate models: description and evaluation in the Community Atmosphere Model CAM5, Geosci. Model Dev., 5, 709-739, doi:10.5194/gmd-5-709-2012, 2012.

Liu, X., Ma, P.-L., Wang, H., Tilmes, S., Singh, B., Easter, R. C., Ghan, S. J., and Rasch, P. J.: Description and evaluation of a new four-mode version of the Modal Aerosol Module (MAM4) within version 5.3 of the Community Atmosphere Model, Geosci. Model Dev., 9, 505-522, doi:10.5194/gmd-9-505-2016, 2016.

Lou, S., Russell, L. M., Yang, Y., Xu, L., Lamjiri, M. A., DeFlorio, M. J., Miller, A. J., Ghan, S. J., Liu, Y., and Singh, B.: Impacts of the East Asian Monsoon on springtime dust concentrations over China, J. Geophys. Res. Atmos., 121, 8137–8152, doi:10.1002/2016JD024758, 2016.

Lu, Z., Zhang, Q., and Streets, D. G.: Sulfur dioxide and primary carbonaceous aerosol emissions in China and India, 1996–2010, Atmos. Chem. Phys., 11, 9839-9864, doi:10.5194/acp-11-9839-2011, 2011.

Ma, P.-L., Gattiker, J. R., Liu, X., and Rasch, P. J.: A novel approach for determining source-receptor relationships in model simulations: a case study of black carbon transport in northern hemisphere winter, Environ. Res. Lett., 8(2), 024042, doi:10.1088/1748-9326/8/2/024042, 2013a.

Ma, P.-L., Rasch, P. J., Wang, H., Zhang, K., Easter, R. C., Tilmes, S., Fast, J. D., Liu, X., Yoon, J.-H., and Lamarque, J.-F.: The role of circulation features on black carbon transport into the Arctic in the Community Atmosphere Model version 5 (CAM5), J. Geophys. Res. Atmos., 118, 4657–4669, doi:10.1002/jgrd.50411, 2013b.

Matsui, H., Koike, M., Kondo, Y., Takegawa, N., Kita, K., Miyazaki, Y., Hu, M., Chang, S.-Y., Blake, D. R., Fast, J. D., Zaveri, R. A., Streets, D. G., Zhang, Q., and Zhu, T.: Spatial and temporal variations of aerosols around Beijing in summer 2006: Model evaluation and source apportionment, J. Geophys. Res., 114, D00G13, doi:10.1029/2008JD010906, 2009.

Matsui, H., Koike, M., Kondo, Y., Oshima, N., Moteki, N., Kanaya, Y., Takami, A., and Irwin, M.: Seasonal variations of Asian black carbon outflow to the Pacific: Contribution from anthropogenic sources in China and biomass burning sources in Siberia and Southeast Asia, J. Geophys. Res. Atmos., 118, 9948–9967, doi:10.1002/jgrd.50702, 2013.

McFarquhar, G., and Wang, H.: Effects of aerosols on trade wind cumuli over the Indian Ocean: Model simulations, Q. J. R. Meteorol. Soc., 132, 821–843, doi:10.1256/qj.04.179, 2006.

Oshima, N., Koike, M., Zhang, Y., Kondo, Y., Moteki, N., Takegawa, N., and Miyazaki, Y.: Aging of black carbon in outflow from anthropogenic sources using a mixing state resolved model: Model development and evaluation, J. Geophys. Res., 114, D06210, doi:10.1029/2008JD010680, 2009.

1014 Oshima, N., Kondo, Y., Moteki, N., Takegawa, N., Koike, M., Kita, K., Matsui, H.,
1015 Kajino, M., Nakamura, H., Jung, J. S., and Kim, Y. J.: Wet removal of black
1016 carbon in Asian outflow: Aerosol Radiative Forcing in East Asia (A-FORCE)
1017 aircraft campaign, J. Geophys. Res., 117, D03204, doi:10.1029/2011jd016552,
1018 2012.
1019
1020 Qian, Y., Flanner, M. G., Leung, L. R., and Wang, W.: Sensitivity studies on the
1021 impacts of Tibetan Plateau snowpack pollution on the Asian hydrological cycle
1022 and monsoon climate, Atmos. Chem. Phys., 11, 1929-1948,
1023 doi:10.5194/acp-11-1929-2011, 2011.
1024
1025 Qian, Y., Wang, H., Zhang, R., Flanner, M. G., and Rasch, P. J.: A sensitivity study on
1026 modeling black carbon in snow and its radiative forcing over the Arctic and
1027 Northern China, Environ. Res. Lett., 9, 064001,
1028 doi:10.1088/1748-9326/9/6/064001, 2014.
1029
1030 Qian, Y., Yasunari, T. J., Doherty, S. J., Flanner, M. G., Lau, W. K. M., Ming, J.,
1031 Wang, H., Wang, M., Warren, S. G., and Zhang, R.: Light-absorbing particles in
1032 snow and ice: Measurement and modeling of climatic and hydrological impact,
1033 *Adv. Atmos. Sci.*, 32(1), 64–91, doi:10.1007/s00376-014-0010-0, 2015.
1034

1035 Qin, Y. and Xie, S. D.: Spatial and temporal variation of anthropogenic black carbon
1036 emissions in China for the period 1980–2009, Atmos. Chem. Phys., 12,
1037 4825-4841, doi:10.5194/acp-12-4825-2012, 2012.
1038
1039 Ramanathan, V., and Carmichael, G.: Global and regional climate changes due to
1040 black carbon, Nat. Geosci., 1, 221-227, doi:10.1038/ngeo156, 2008.
1041
1042 Rienecker, M. M., Suarez, M. J., Gelaro, R., Todling, R., Bacmeis- ter, J., Liu, R.,
1043 Bosilovich, M. G., Schubert, S. D., Takacs, L., Kim, G-K, Bloom, S., Chen, J.,
1044 Collins, D., Conaty, A., da Silva, A., Gu, W., Joiner, J., Koster, R. D., Lucchesi,
1045 R., Molod, A., Owens, T., Pawson, S., Pegion, P., Redder, C. R., Reichle, R.,
1046 Robertson, F. R., Ruddick, A. G., Sienkiewicz, M., and Woollen, J.: MERRA:
1047 NASA's Modern-Era Retrospective Analysis for Research and Applications, J.
1048 Climate, 24, 3624–3648, 2011.
1049
1050 Schuster, G. L., Dubovik, O., Arola, A., Eck, T. F., and Holben, B. N.: Remote sensing
1051 of soot carbon – Part 2: Understanding the absorption Ångström exponent,
1052 Atmos. Chem. Phys., 16, 1587-1602, doi:10.5194/acp-16-1587-2016, 2016.
1053
1054 Shindell, D., et al. (2012), Simultaneously mitigating near-term climate change and
1055 improving human health and food security, Science, 335(6065), 183-189,
1056 doi:10.1126/science.1210026.

Shindell, D., Kuylenstierna, J. C. I., Vignati, E., van Dingenen, R., Amann, M., Klimont, Z., Anenberg, S. C., Muller, N., Janssens- Maenhout, G., Raes, F., Schwartz, J., Faluvegi, G., Pozzoli, L., Kupiainen, K., Höglund-Isaksson, L., Emberson, L., Streets, D., Ramanathan, V., Hicks, K., Oanh, N. T. K., Milly, G., Williams, M., Demkine, V., and Fowler, D.: Simultaneously Mitigating Near-Term Climate Change and Improving Human Health and Food Security, Science, 335, 183–189, doi:10.1126/science.1210026, 2012.

Smith, S. J., and Mizrahi, A.: Near-term climate mitigation by short-lived forcers, Proc. Natl. Acad. Sci, 110(35), 14202-14206, doi:10.1073/pnas.1308470110, 2013.

Sun, Y., Jiang, Q., Wang, Z., Fu, P., Li, J., Yang, T., and Yin, Y.: Investigation of the sources and evolution processes of severe haze pollution in Beijing in January 2013, J. Geophys. Res. Atmos., 119, 4380–4398, doi:10.1002/2014JD021641, 2014.

Wang, H., Easter, R. C., Rasch, P. J., Wang, M., Liu, X., Ghan, S. J., Qian, Y., Yoon, J.-H., Ma, P.-L., and Vinoj, V.: Sensitivity of remote aerosol distributions to representation of cloud–aerosol interactions in a global climate model, Geosci. Model Dev., 6, 765-782, doi:10.5194/gmd-6-765-2013, 2013.

1079 Wang, H., Rasch, P. J., Easter, R. C., Singh, B., Zhang, R., Ma, P.-L., Qian, Y., Ghan,
1080 S. J., and Beagley, N.: Using an explicit emission tagging method in global
1081 modeling of source-receptor relationships for black carbon in the Arctic:
1082 Variations, sources, and transport pathways, J. Geophys. Res. Atmos., 119,
1083 12,888–12,909, doi:10.1002/ 2014JD022297, 2014.
1084
1085 Wang, L. T., Wei, Z., Yang, J., Zhang, Y., Zhang, F. F., Su, J., Meng, C. C., and
1086 Zhang, Q.: The 2013 severe haze over southern Hebei, China: model evaluation,
1087 source apportionment, and policy implications, Atmos. Chem. Phys., 14,
1088 3151-3173, doi:10.5194/acp-14-3151-2014, 2014.
1089
1090 Wang, M., Ghan, S., Ovchinnikov, M., Liu, X., Easter, R., Kassianov, E., Qian, Y., and
1091 Morrison, H.: Aerosol indirect effects in a multi-scale aerosol-climate model
1092 PNNL-MMF, Atmos. Chem. Phys., 11, 5431-5455,
1093 doi:10.5194/acp-11-5431-2011, 2011.
1094
1095 Wang, Q., Jacob, D. J., Spackman, J. R., Perring, A. E., Schwarz, J. P., Moteki, N.,
1096 Marais, E. A., Ge, C., Wang, J., and Bar- rett, S. R. H.: Global budget and
1097 radiative forcing of black car- bon aerosol: Constraints from pole-to-pole (HIPPO)
1098 observa- tions across the Pacific, J. Geophys. Res.-Atmos., 119, 195–206,
1099 doi:10.1002/2013jd020824, 2014.
1100

1101 Wang, R., Tao, S., Balkanski, Y., Ciais, P., Boucher, O., Liu, J., Piao, S., Shen, H.,
1102 Vuolo, M. R., and Valari, M.: Exposure to ambient black carbon derived from a
1103 unique inventory and high- resolution model, P. Natl. Acad. Sci. USA, 111, 2459–
1104 2463, 2014.
1105
1106 Wang, X., Wang, Y., Hao, J., Kondo, Y., Irwin, M., Munger, J. W., and Zhao, Y.:
1107 Top-down estimate of China's black carbon emissions using surface
1108 observations: Sensitivity to observation representativeness and transport model
1109 error, J. Geophys. Res. Atmos., 118, 5781–5795, doi:10.1002/jgrd.50397, 2013.
1110
1111 Wu, J., Fu, C., Xu, Y., Tang, J. P., Wang, W., and Wang, Z.: Simulation of direct
1112 effects of black carbon aerosol on temperature and hydrological cycle in Asia by a
1113 Regional Climate Model, Meteorol. Atmos. Phys., 100(1), 179–193,
1114 doi:10.1007/s00703-008-0302-y, 2008.
1115
1116 Yang, Y., Liao, H., and Lou, S.: Decadal trend and interannual variation of outflow of
1117 aerosols from East Asia: Roles of variations in meteorological parameters and
1118 emissions, Atmos. Environ., 100, 141-153, doi:10.1016/j.atmosenv.2014.11.004,
1119 2015.
1120

1121 Yang, Y., Liao, H., and Lou, S.: Increase in winter haze over eastern China in recent
1122 decades: Roles of variations in meteorological parameters and anthropogenic
1123 emissions, J. Geophys. Res. Atmos., 121, doi:10.1002/2016JD025136, 2016.
1124
1125 Yu, H., Remer, L. A., Chin, M., Bian, H., Kleidman, R. G., and Diehl, T.: A
1126 satellite-based assessment of transpacific transport of pollution aerosol, J.
1127 Geophys. Res., 113, D14S12, doi:10.1029/2007JD009349, 2008.
1128
1129 Zhang, K., Wan, H., Liu, X., Ghan, S. J., Kooperman, G. J., Ma, P.-L., Rasch, P. J.,
1130 Neubauer, D., and Lohmann, U.: Technical Note: On the use of nudging for
1131 aerosol–climate model intercomparison studies, Atmos. Chem. Phys., 14,
1132 8631-8645, doi:10.5194/acp-14-8631-2014, 2014.
1133
1134 Zhang, L. M., Gong, S. L., Padro, J., and Barrie, L.: A size-segregated particle dry
1135 deposition scheme for an atmospheric aerosol module, Atmos. Environ., 35,
1136 549-560, doi:10.1016/S1352-2310(00)00326-5, 2001.
1137
1138 Zhang, Q., Streets, D. G., Carmichael, G. R., He, K. B., Huo, H., Kannari, A., Klimont,
1139 Z., Park, I. S., Reddy, S., Fu, J. S., Chen, D., Duan, L., Lei, Y., Wang, L. T., and
1140 Yao, Z. L.: Asian emissions in 2006 for the NASA INTEX-B mission, Atmos.
1141 Chem. Phys., 9, 5131-5153, doi:10.5194/acp-9-5131-2009, 2009.
1142

1143 Zhang, R. H., Li, Q., and Zhang, R. N.: Meteorological conditions for the persistent
1144 severe fog and haze event over eastern China in January 2013, Sci. China Earth
1145 Sci., 57(1), 26–35, doi:10.1007/s11430-013-4774-3, 2014.
1146
1147 Zhang, R., Wang, H., Hegg, D. A., Qian, Y., Doherty, S. J., Dang, C., Ma, P.-L.,
1148 Rasch, P. J., and Fu, Q.: Quantifying sources of black carbon in western North
1149 America using observationally based analysis and an emission tagging technique
1150 in the Community Atmosphere Model, Atmos. Chem. Phys., 15, 12805-12822,
1151 doi:10.5194/acp-15-12805-2015, 2015a.
1152
1153 Zhang, R., Wang, H., Qian, Y., Rasch, P. J., Easter, R. C., Ma, P.-L., Singh, B.,
1154 Huang, J., and Fu, Q.: Quantifying sources, transport, deposition, and radiative
1155 forcing of black carbon over the Himalayas and Tibetan Plateau, Atmos. Chem.
1156 Phys., 15, 6205-6223, doi:10.5194/acp-15-6205-2015, 2015b.
1157
1158 Zhang, X. Y., Wang, Y. Q., Zhang, X. C., Guo, W., and Gong, S. L.: Carbonaceous
1159 aerosol composition over various regions of China during 2006, J. Geophys.
1160 Res., 113, D14111, doi:10.1029/2007JD009525, 2008.
1161
1162 Zhang, X. Y., Wang, Y. Q., Niu, T., Zhang, X. C., Gong, S. L., Zhang, Y. M., and Sun,
1163 J. Y.: Atmospheric aerosol compositions in China: spatial/temporal variability,
1164 chemical signature, regional haze distribution and comparisons with global

1165 aerosols, Atmos. Chem. Phys., 12, 779-799, doi:10.5194/acp-12-779-2012,
1166 2012.
1167
1168 Zhang, Y.-L., Huang, R.-J., El Haddad, I., Ho, K.-F., Cao, J.-J., Han, Y., Zotter, P.,
1169 Bozzetti, C., Daellenbach, K. R., Canonaco, F., Slowik, J. G., Salazar, G.,
1170 Schwikowski, M., Schnelle-Kreis, J., Abbaszade, G., Zimmermann, R.,
1171 Baltensperger, U., Prévôt, A. S. H., and Szidat, S.: Fossil vs. non-fossil sources of
1172 fine carbonaceous aerosols in four Chinese cities during the extreme winter haze
1173 episode of 2013, Atmos. Chem. Phys., 15, 1299-1312,
1174 doi:10.5194/acp-15-1299-2015, 2015.
1175
1176 Zhao, Y., Zhang, J., and Nielsen, C. P.: The effects of recent control policies on
1177 trends in emissions of anthropogenic atmospheric pollutants and CO2 in China,
1178 Atmos. Chem. Phys., 13, 487-508, doi:10.5194/acp-13-487-2013, 2013.
1179
1180 Zhuang, B. L., Jiang, F., Wang, T. J., Li, S., and Zhu, B.: Investigation on the direct
1181 radiative effect of fossil fuel black-carbon aerosol over China, Theor. Appl.
1182 Climatol., 104(3), 301–312, doi:10.1007/s00704-010-0341-4, 2011.
1183
1184 Zhuang, B. L., Liu, Q., Wang, T. J., Yin, C. Q., Li, S., Xie, M., Jiang, F., and Mao, H.
1185 T.: Investigation on semi-direct and indirect climate effects of fossil fuel black

carbon aerosol over China, Theor. Appl. Climatol., 114 (3), 651–672, doi:10.1007/s00704-013-0862-8, 2013.

Zhuang, B. L., Wang, T. J., Liu, J., Li, S., Xie, M., Yang, X. Q., Fu, C. B., Sun, J. N., Yin, C. Q., Liao, J. B., Zhu, J. L., and Zhang, Y.: Continuous measurement of black carbon aerosol in urban Nanjing of Yangtze River Delta, China, Atmos. Environ., 89, 415–424, doi:10.1016/j.atmosenv.2014.02.052, 2014.

Figure Captions

Figure 1. (a) Spatial distribution of annual mean total emissions (anthropogenic plus biomass burning, units: g C m^{-2} yr^{-1}) of black carbon (BC) averaged over 2010–2014. The geographical BC source regions are selected as North China (NC, 109°E–east boundary, 30°–41°N), South China (SC, 109°E–east boundary, south boundary–30°N), Southwest China (SW, 100°–109°N, south boundary–32°N), Central-West China (CW, 100°–109°N, 32°N–north boundary), Northeast China (NE, 109°E–east boundary, 41°N–north boundary), Northwest China (NW, west boundary–100°E, 36°N–north boundary), and Tibetan Plateau (TP, west boundary–100°E, south boundary–36°N) in China and regions outside of China (RW, rest of the world). (b) Seasonal mean total emissions (units: Gg C, Gg = 10^9g) of BC from the seven BC source regions in China and emissions from rest of East Asia (REA, with China excluded), South Asia (SAS), Southeast Asia (SEA), and Russia/Belarussia/Ukraine (RBU).

Figure 2. Simulated seasonal mean near-surface concentrations (left, units: μg m^{-3}) and column burden (right, units: mg m^{-2}) of BC in December-January-February (DJF), March-April-May (MAM), June-July-August (JJA), and September-October-November (SON).

Figure 3. Comparisons of observed and modeled seasonal mean (a) near-surface concentrations (units: μg m^{-3}) and (b) aerosol absorption optical depth (AAOD) of BC in China. Solid lines mark the 1:1 ratios and dashed lines mark the 1:3 and 3:1 ratios. Observed BC concentrations were taken between 2006 and 2007 at 14 sites of the China Meteorological Administration (CMA) Atmosphere Watch Network (CAWNET) (Zhang et al., 2012). Observed AAOD of BC are obtained by removing dust AAOD from total AAOD at 10 sites of the Aerosol Robotic Network (AERONET) (Holben et al., 2001), following Bond et al. (2013). The observed AAOD are averaged over years of 2005–2014 with data available. Correlation coefficient (R) and normalized mean

bias (NMB) between observation and simulation are shown on top left of each panel. NMB = 100%× $\sum(M_i - O_i) / \sum O_i$, where M_i and O_i are the modeled and observed values at site i, respectively. Site locations are shown in Figure S1a.

Figure 4. Spatial distribution of seasonal mean AAOD of total aerosols (left) and Aerosol Index (AI) derived from Ozone Monitoring Instrument (OMI) measurements over years of 2010–2014 (right).

Figure 5. Spatial distribution of seasonal mean near-surface concentrations of BC (μg m^{-3}) originating from the seven source regions in China (NC, SC, SW, CW, NE, NW, and TP), marked with black outlines, and sources outside China (RW). Regionally averaged BC in China contributed by individual source regions is shown at the bottom right of each panel.

Figure 6. Spatial distribution of relative contributions (%) to seasonal mean near-surface BC concentrations from each of the tagged source regions.

Figure 7. Relative contributions (%) from the tagged source regions (denoted by colors) to regional mean surface concentrations of BC over seven receptor regions in China (NC, SC, SW, CW, NE, NW, and TP) and China (seven regions combined, CN) in different seasons. The receptor regions are marked on the horizontal axis in each panel.

Figure 8. Composite differences in winds at 850 hPa (m s^{-1}) and near-surface BC concentrations (μg m^{-3}) between polluted and normal days in DJF.

Figure 9. Composite differences in surface BC concentrations (μg m^{-3}) averaged over receptor regions (marked on the horizontal axis) over eastern and central China between polluted and normal days in DJF originating from individual sources regions (bars in each column).

Figure 10. Spatial distribution of (a, b) column burden (mg m^{-2}) and (c, d) near-surface concentrations (μg m^{-3}) of BC originating from total emissions inside (CN) and outside China (RW), respectively, in March-April-May (MAM). The black solid lines over western (150°E, 20°–60°N) Pacific in panel (a) mark the cross-sections used to quantify outflow of BC from East Asia. The box over western United States (125°–105°W, 30°–50°N) in panel (c) is used to quantify BC concentrations attributed to sources from China.

Figure 11. Spatial distribution of annual mean direct radiative forcing of BC (W m^{-2}) at the top of the atmosphere originating from the tagged BC source regions in China (NC, SC, SW, CW, NE, NW, and TP) and source outside China (RW). Regionally averaged forcing in China contributed by individual source regions is shown at the bottom right of each panel.

Figure 12. (a, c) BC seasonal DRF averaged over China as a function of BC emission fraction (the ratio of regional emission to the total emission over China and global, respectively, unit: %) for each of the tagged regions. (b, d) Seasonal DRF efficiency of BC (W m^{-2} Tg^{-1}) for each of the tagged source regions over China and globally, respectively. The efficiency is defined as the DRF divided by the corresponding scaled annual emission (seasonal emission multiplied by 4). Error bars indicate 1-σ of mean values during years 2010–2014.

Figure 13. Seasonal (a, b) near-surface concentration (μg m^{-3} Tg^{-1}) and (c, d) column burden (mg m^{-2} Tg^{-1}) efficiency of BC for each of the tagged source regions over China and globally, respectively.

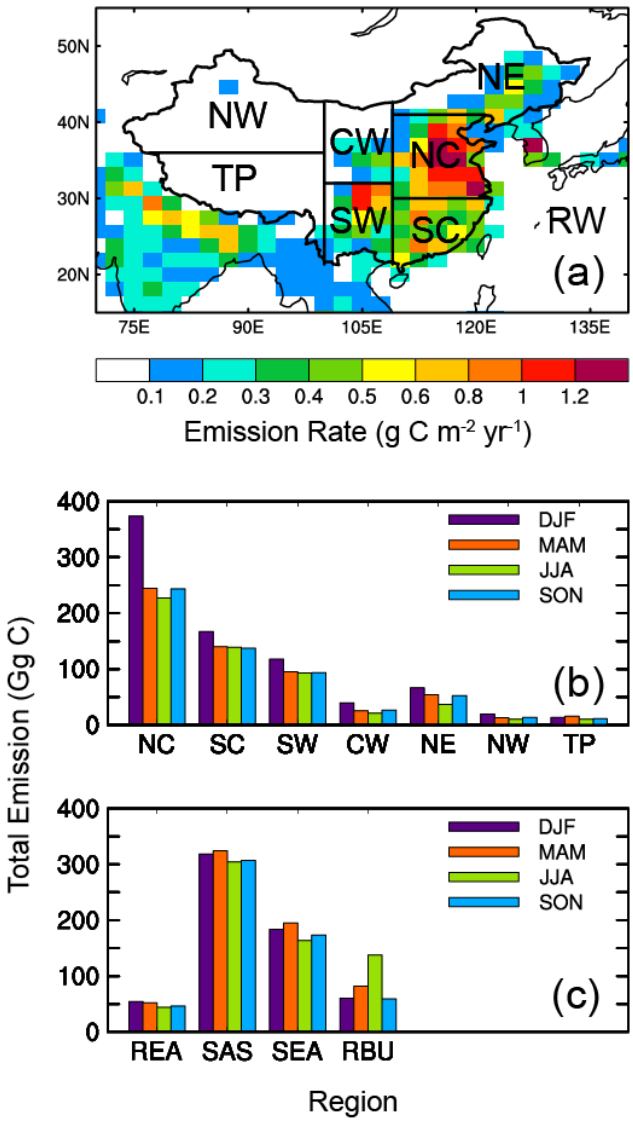

Figure 1. (a) Spatial distribution of annual mean total emissions (anthropogenic plus biomass burning, units: g C m^{-2} yr^{-1}) of black carbon (BC) averaged over 2010–2014. The geographical BC source regions are selected as North China (NC, 109°E–east boundary, 30°–41°N), South China (SC, 109°E–east boundary, south boundary–30°N), Southwest China (SW, 100°–109°N, south boundary–32°N), Central-West China (CW, 100°–109°N, 32°N–north boundary), Northeast China (NE, 109°E–east boundary, 41°N–north boundary), Northwest China (NW, west boundary–100°E, 36°N–north boundary), and Tibetan Plateau (TP, west boundary–100°E, south boundary–36°N) in China and regions outside of China (RW, rest of the world). (b) Seasonal mean total emissions (units: Gg C, Gg = 10^9g) of BC from the seven BC

source regions in China and (c) emissions from rest of East Asia (REA, with China excluded), South Asia (SAS), Southeast Asia (SEA), and Russia/Belarussia/Ukraine (RBU).

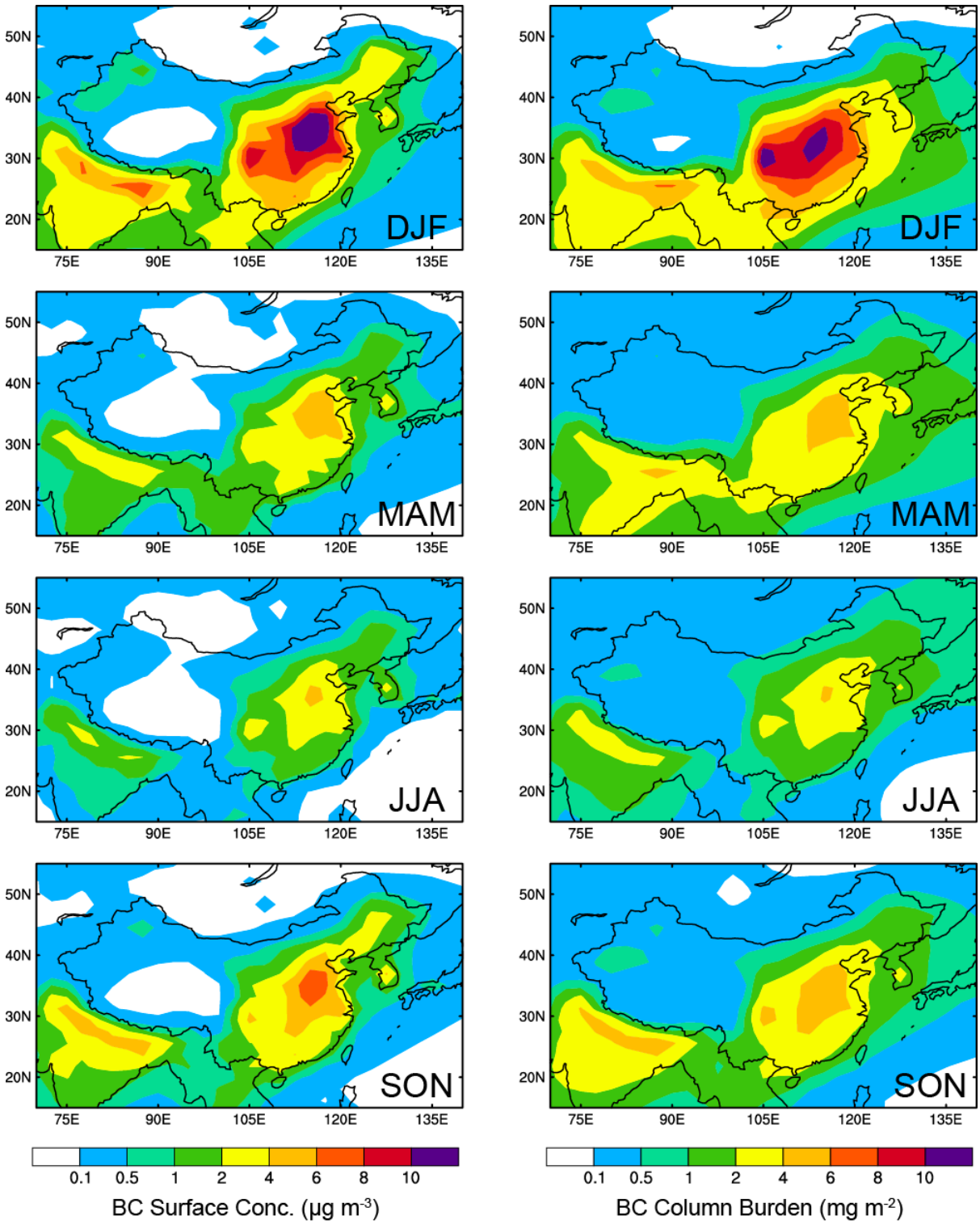

Figure 2. Simulated seasonal mean near-surface concentrations (left, units: μg m^{-3}) and column burden (right, units: mg m^{-2}) of BC in December-January-February (DJF), March-April-May (MAM), June-July-August (JJA), and September-October-November (SON).

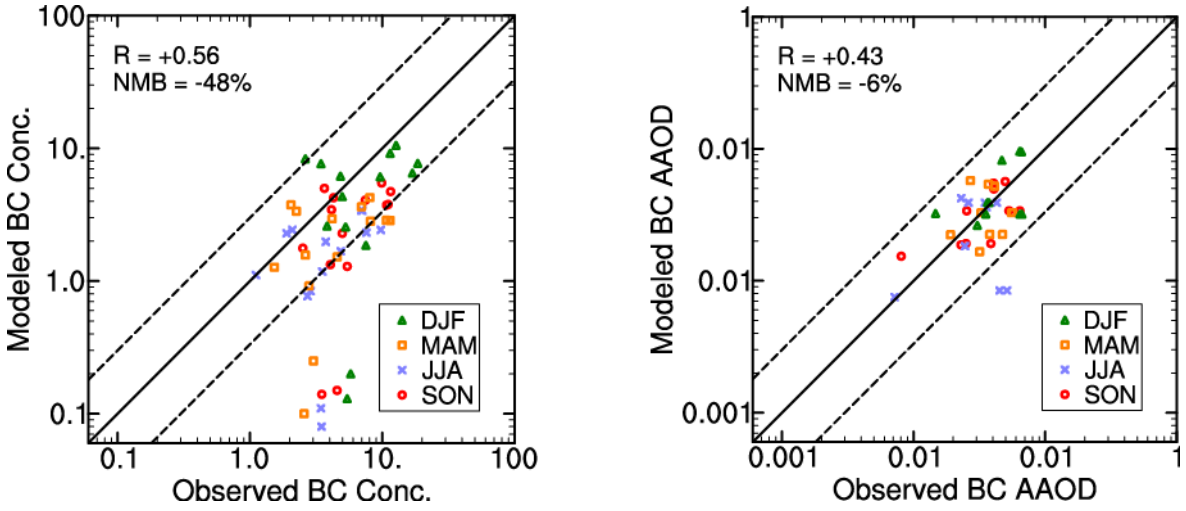

Figure 3. Comparisons of observed and modeled seasonal mean (a) near-surface concentrations (units: μg m^{-3}) and (b) aerosol absorption optical depth (AAOD) of BC in China. Solid lines mark the 1:1 ratios and dashed lines mark the 1:3 and 3:1 ratios. Observed BC concentrations were taken between 2006 and 2007 at 14 sites of the China Meteorological Administration (CMA) Atmosphere Watch Network (CAWNET) (Zhang et al., 2012). Observed AAOD of BC are obtained by removing dust AAOD from total AAOD at 10 sites of the Aerosol Robotic Network (AERONET) (Holben et al., 2001), following Bond et al. (2013). The observed AAOD are averaged over years of 2010–2014 over 7 sites and 2005–2010 over 3 sites with data available. Correlation coefficient (R) and normalized mean bias (NMB) between observation and simulation are shown on top left of each panel. NMB = $100\% \times \sum(M_i - O_i) / \sum O_i$, where M_i and O_i are the modeled and observed values at site i, respectively. Site locations are shown in Figure S1a.

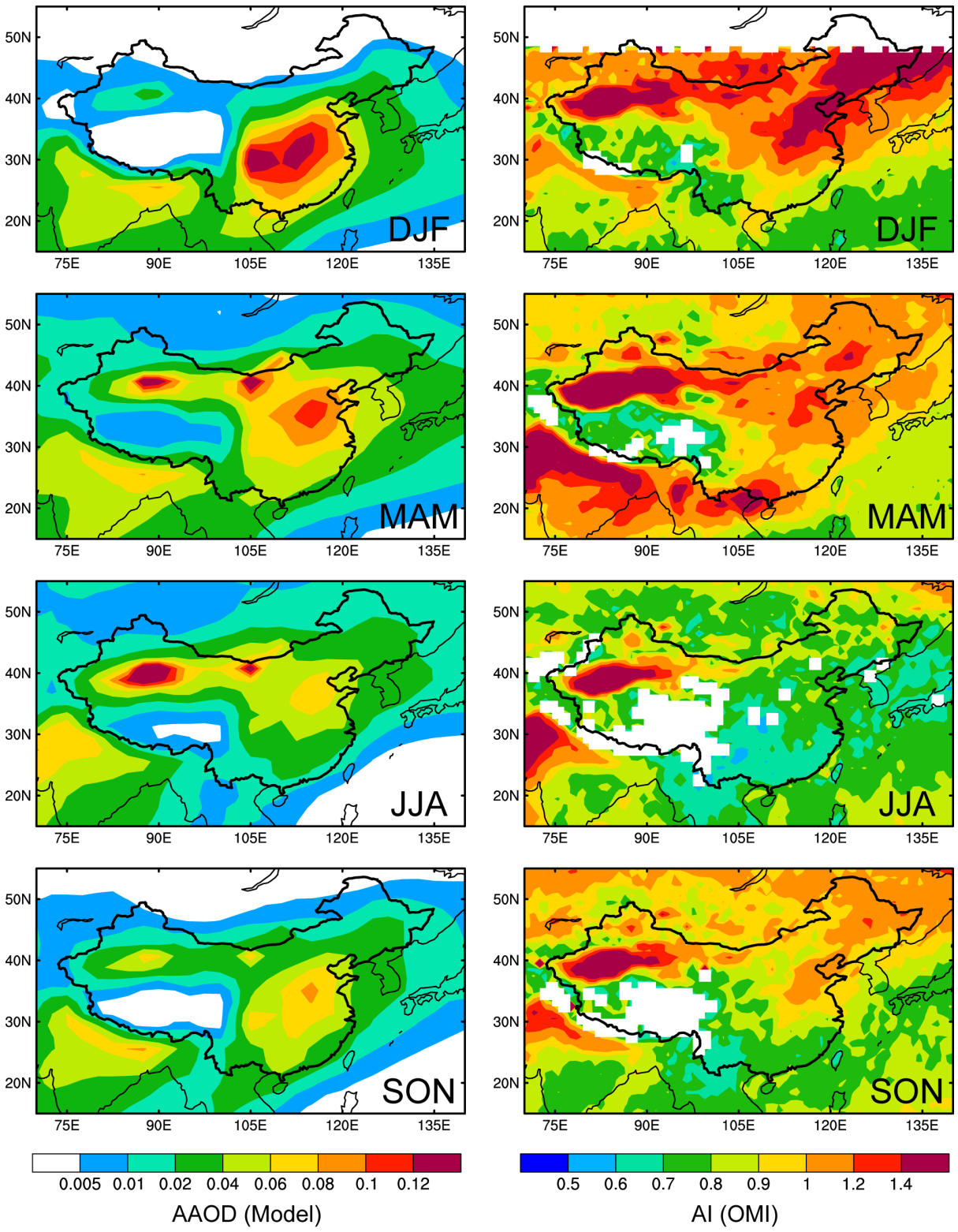

Figure 4. Spatial distribution of seasonal mean AAOD of total aerosols (left) and Aerosol Index (AI) derived from Ozone Monitoring Instrument (OMI) measurements over years of 2010–2014 (right).

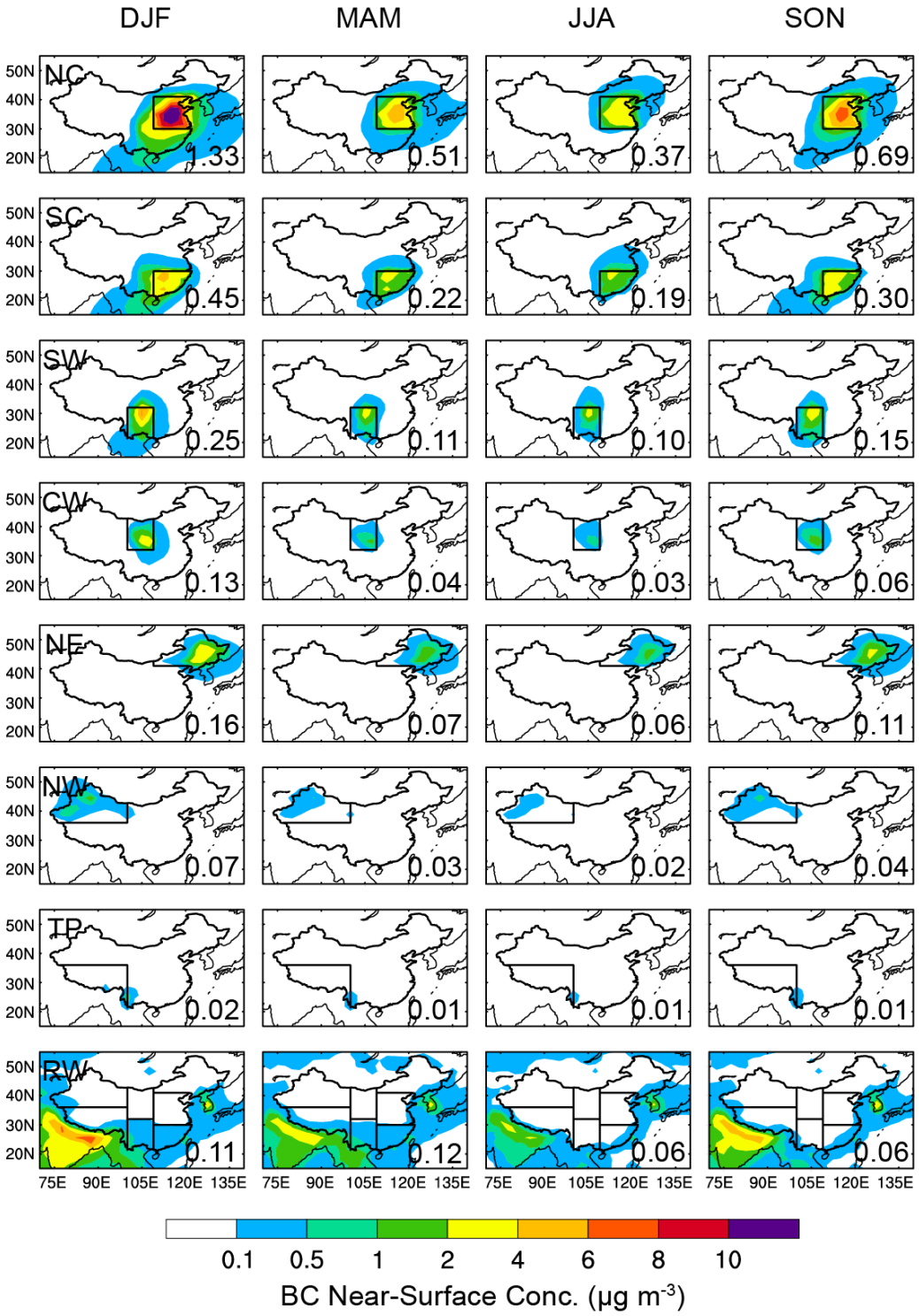

Figure 5. Spatial distribution of seasonal mean near-surface concentrations of BC (μg m^{-3}) originating from the seven source regions in China (NC, SC, SW, CW, NE, NW, and TP), marked with black outlines, and sources outside China (RW). Regionally averaged BC in China contributed by individual source regions is shown at the bottom right of each panel.

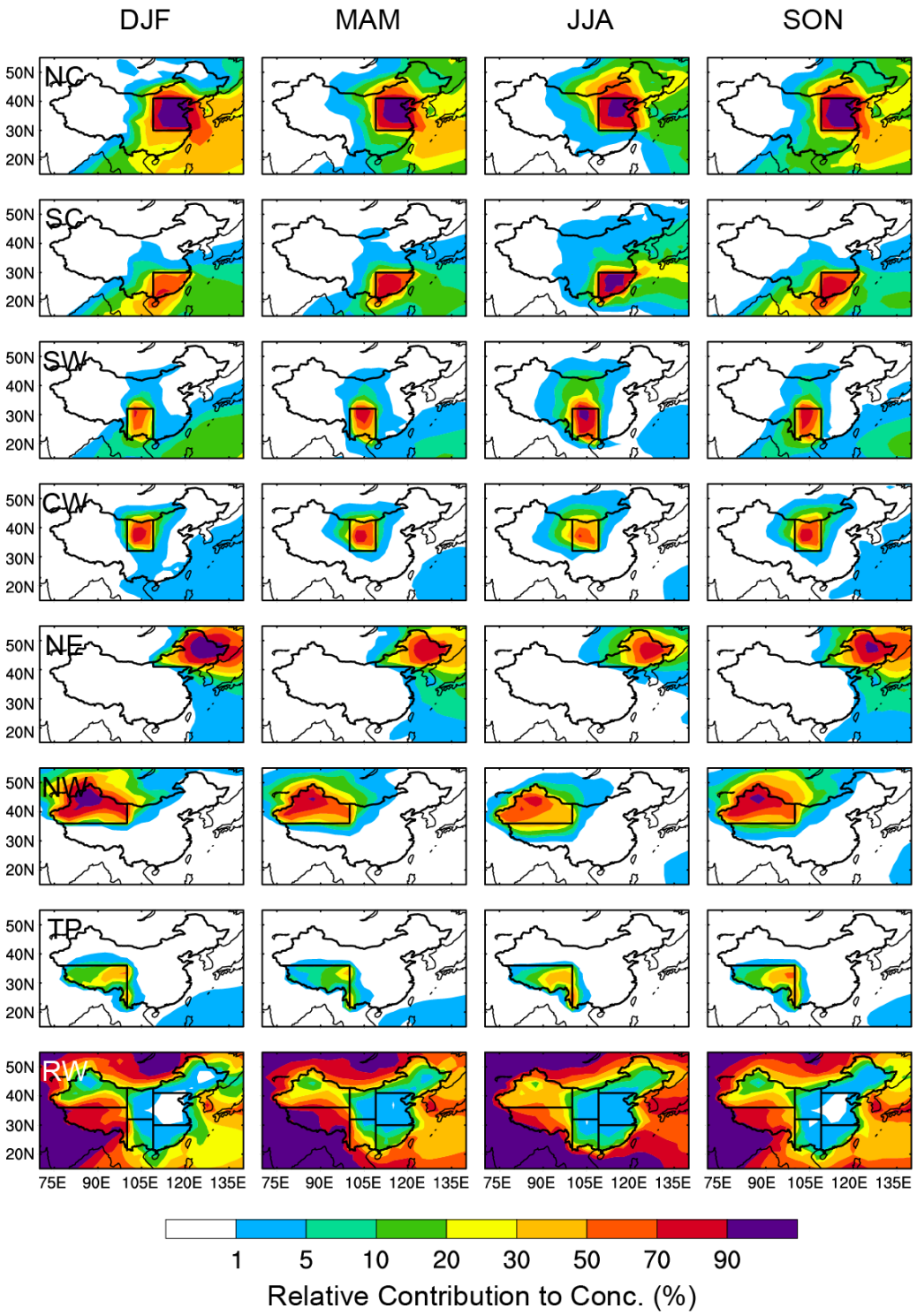

Figure 6. Spatial distribution of relative contributions (%) to seasonal mean near-surface BC concentrations from each of the tagged source regions.

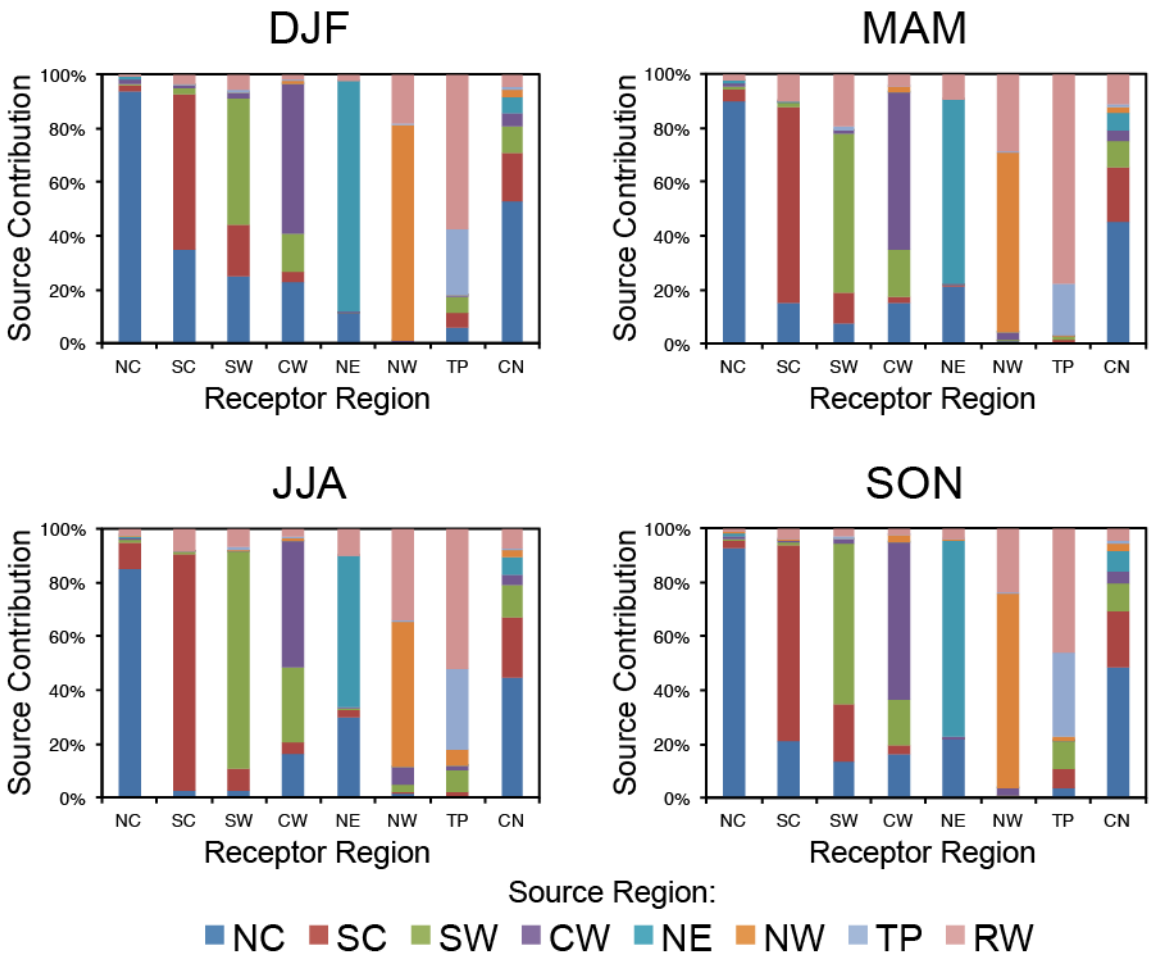

Figure 7. Relative contributions (%) from the tagged source regions (denoted by colors) to regional mean surface concentrations of BC over seven receptor regions in China (NC, SC, SW, CW, NE, NW, and TP) and China (seven regions combined, CN) in different seasons. The receptor regions are marked on the horizontal axis in each panel.

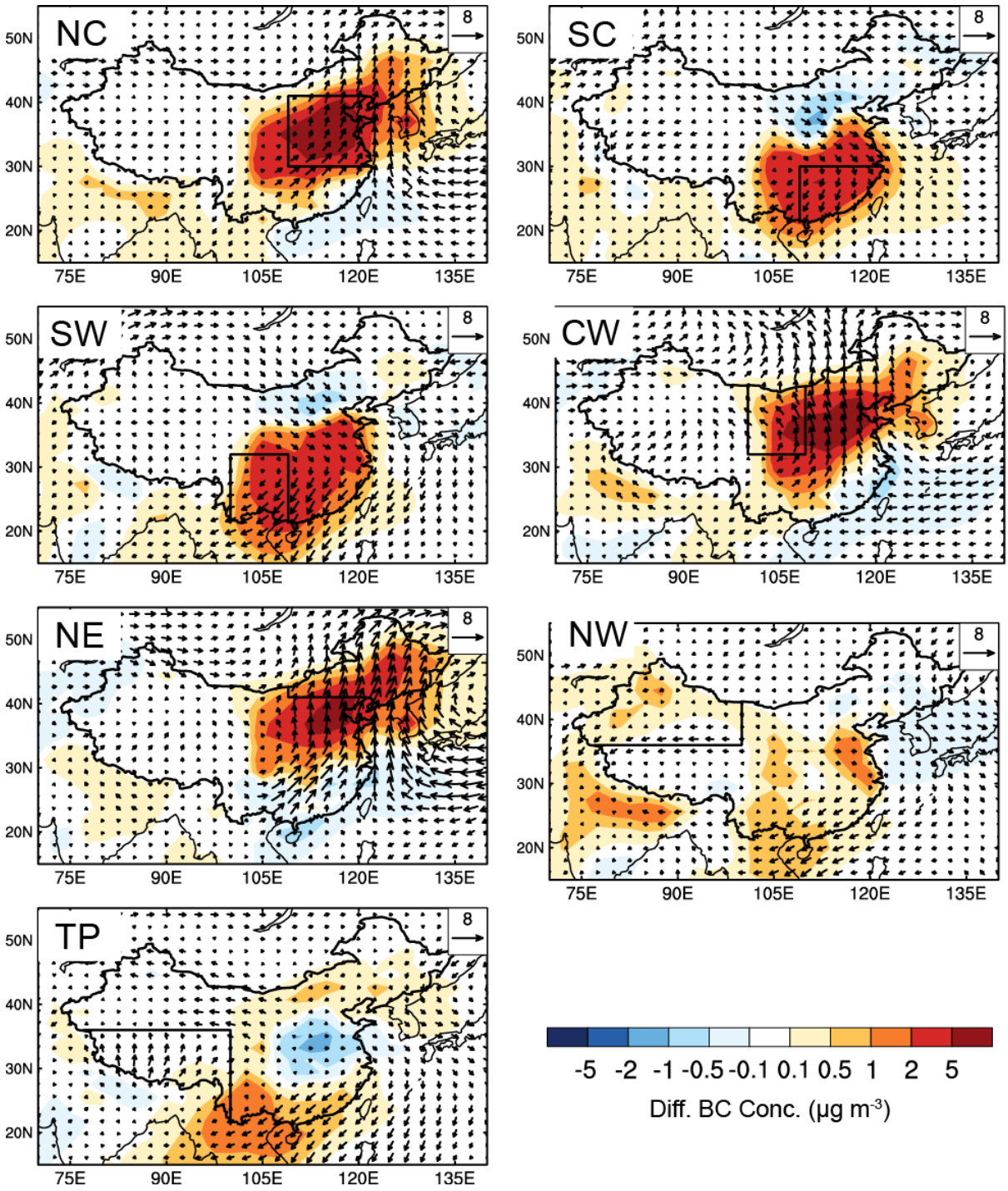

Figure 8. Composite differences in winds at 850 hPa (m s^{-1}) and near-surface BC concentrations (μg m^{-3}) between polluted and normal days in DJF.

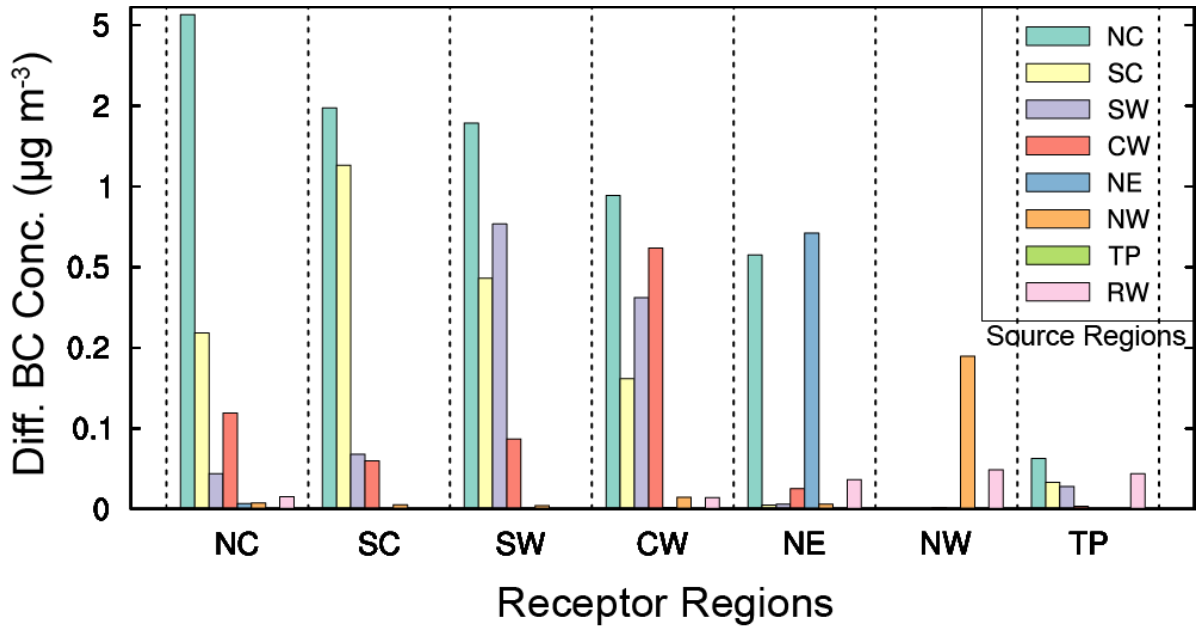

Figure 9. Composite differences in surface BC concentrations (μg m^{-3}) averaged over receptor regions (marked on the horizontal axis) over eastern and central China between polluted and normal days in DJF originating from individual sources regions (bars in each column).

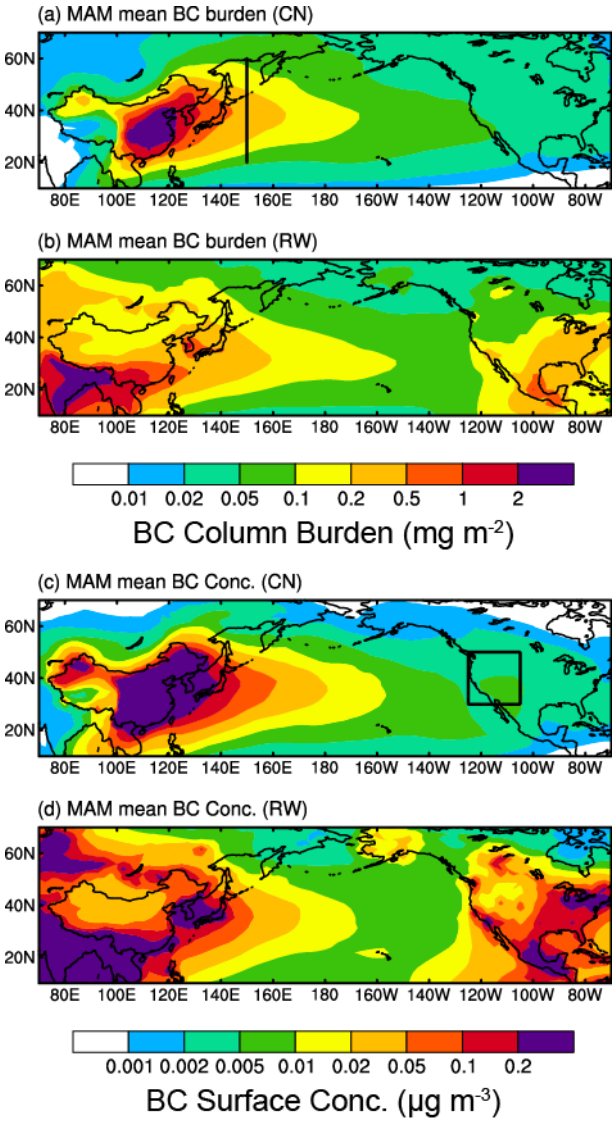

1361
1362

1363 **Figure 10.** Spatial distribution of (a, b) column burden (mg m^{-2}) and (c, d)
1364 near-surface concentrations (μg m^{-3}) of BC originating from total emissions inside
1365 (CN) and outside China (RW), respectively, in March-April-May (MAM). The black
1366 solid lines over western (150°E, 20°–60°N) Pacific in panel (a) mark the
1367 cross-sections used to quantify outflow of BC from East Asia. The box over western
1368 United States (125°–105°W, 30°–50°N) in panel (c) is used to quantify BC
1369 concentrations attributed to sources from China.

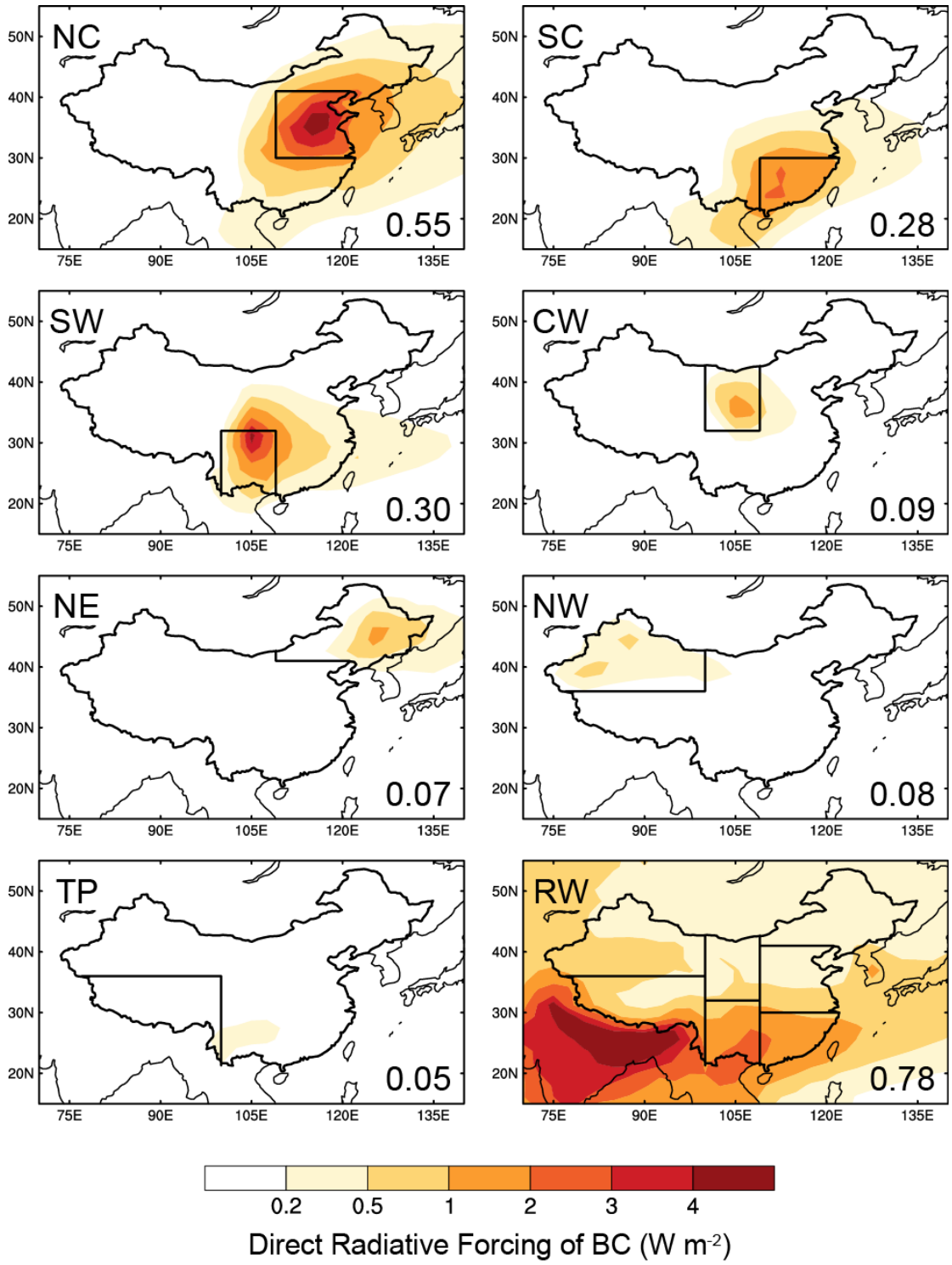

Figure 11. Spatial distribution of annual mean direct radiative forcing (DRF) of BC (W m^{-2}) at the top of the atmosphere originating from the tagged BC source regions in China (NC, SC, SW, CW, NE, NW, and TP) and source outside China (RW). Regionally averaged forcing in China contributed by individual source regions is shown at the bottom right of each panel.

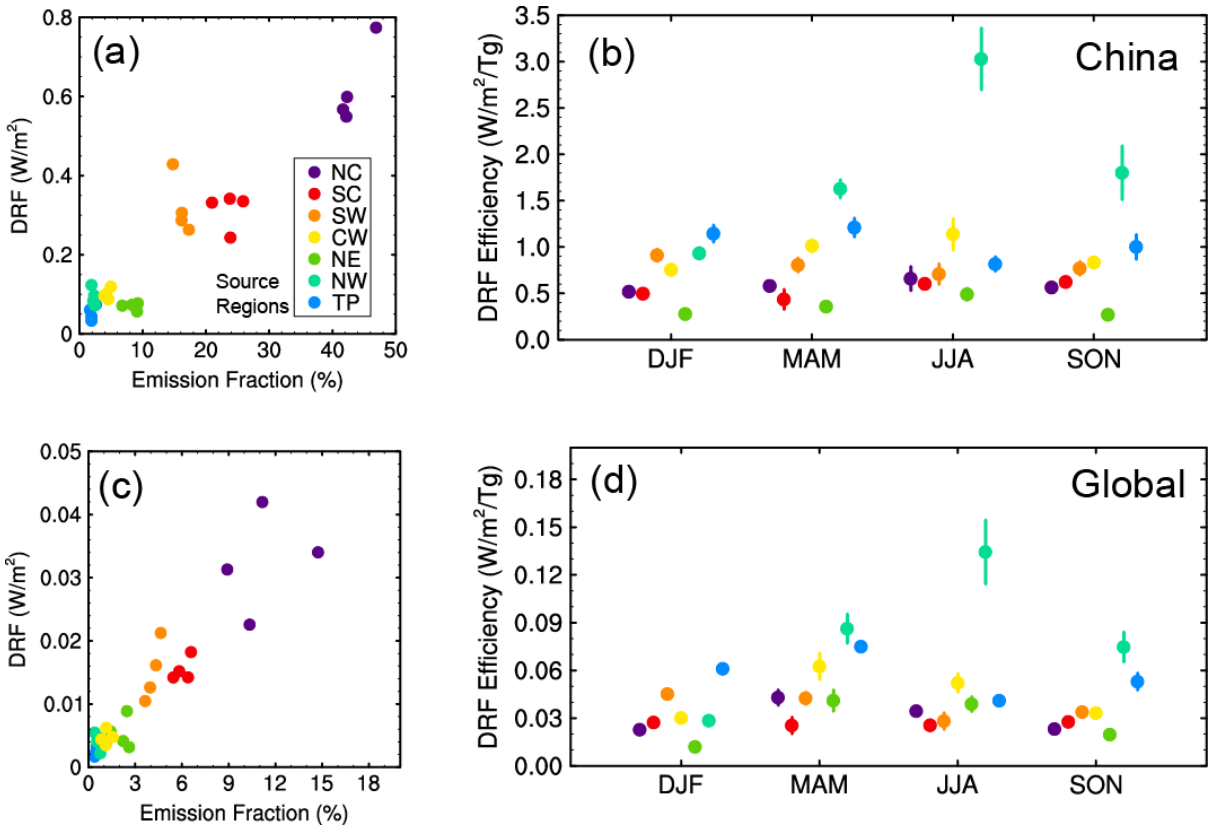

Figure 12. (a, c) BC seasonal DRF averaged over China as a function of BC emission fraction (the ratio of regional emission to the total emission over China and global, respectively, unit: %) for each of the tagged regions. (b, d) Seasonal DRF efficiency of BC (W m^{-2} Tg^{-1}) for each of the tagged source regions over China and globally, respectively. The efficiency is defined as the DRF divided by the corresponding scaled annual emission (seasonal emission multiplied by 4). Error bars indicate 1-σ of mean values during years 2010–2014.

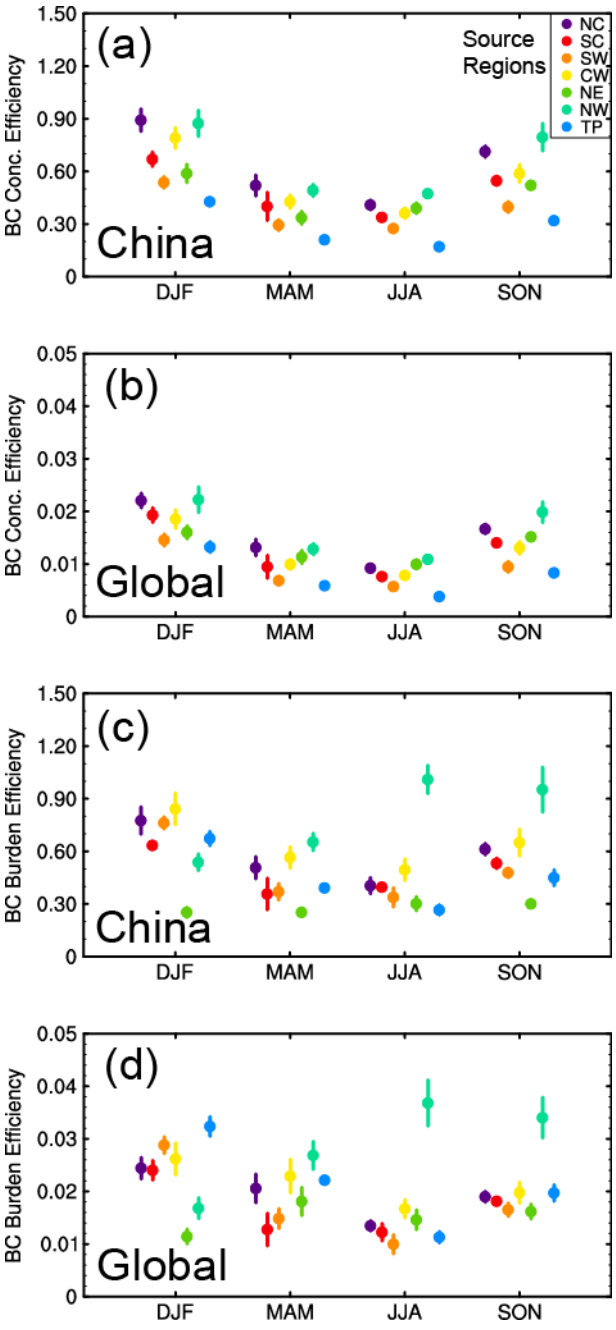

1387

1388

1389 **Figure 13.** Seasonal (a, b) near-surface concentration (μg m^{-3} Tg^{-1}) and (c, d) column

1390 burden (mg m^{-2} Tg^{-1}) efficiency of BC for each of the tagged source regions over

1391 China and globally, respectively.